Immunization with synthetic SARS-CoV-2 S glycoprotein virus-like particles protects macaques from infection

Guidenn Sulbaran, Pauline Maisonnasse, Axelle Amen, Gregory Effantin, Delphine Guilligay, Nathalie Dereuddre-Bosquet, Judith Burger, Meliawati Poniman, Marloes Grobben, Marlyse Buisson, et al.

Cell Reports
Medicine

Article

Immunization with synthetic SARS-CoV-2 S glycoprotein virus-like particles protects macaques from infection

Graphical abstract

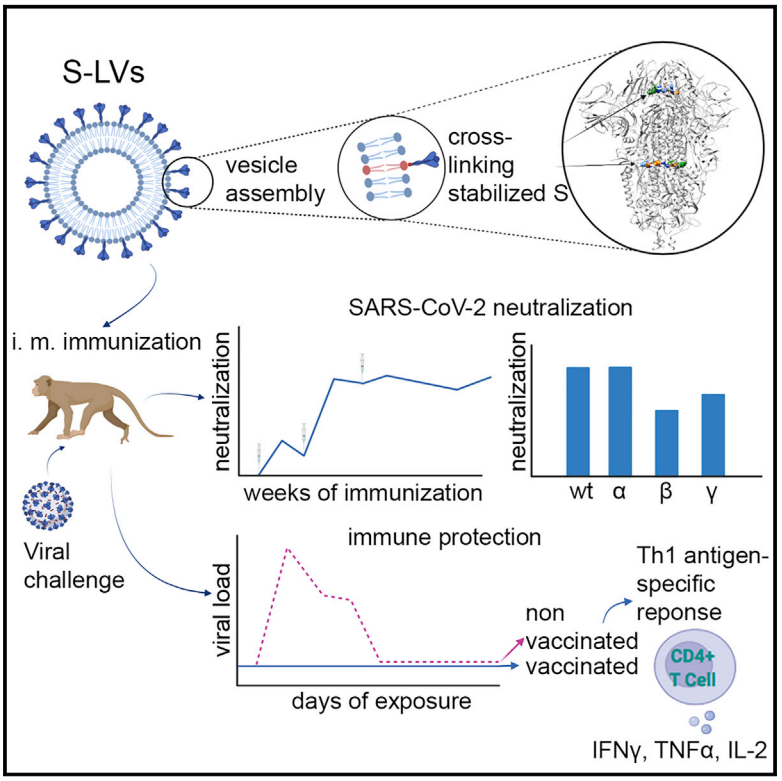

Highlights

- S glycoprotein formaldehyde cross-linking stabilizes S in the prefusion conformation
- Vaccination of cynomolgus macaques with S lipid particles induces neutralization
- Vaccination protects macaques against a SARS-CoV-2 challenge
- Sterilizing protection correlates with nasopharyngeal anti-S IgG and IgA titers

Authors

Guidenn Sulbaran, Pauline Maisonnasse, Axelle Amen, ..., Pascal Poignard, Roger Le Grand, Winfried Weissenhorn

Correspondence

winfried.weissenhorn@ibs.fr (W.W.), roger.le-grand@cea.fr (R.L.G.)

In brief

Sulbaran et al. find that formaldehyde cross-linked S lipid nanoparticles induce potent neutralizing antibody titers upon cynomolgus macaque vaccination. Notably, vaccinated animals develop sterilizing immunity as highlighted upon virus challenge. Thus, the study provides a path to induce sterilizing immunity correlating with mucosal immune responses, which are desired to prevent virus spreading.

Sulbaran et al., 2022, Cell Reports Medicine 3, 100528
February 15, 2022
https://doi.org/10.1016/j.xcrm.2022.100528

CellPress

Cell Reports Medicine

CellPress
OPEN ACCESS

Article

Immunization with synthetic SARS-CoV-2 S glycoprotein virus-like particles protects macaques from infection

Guidenn Sulbaran,[1,7] Pauline Maisonnasse,[2,7] Axelle Amen,[1] Gregory Effantin,[1] Delphine Guilligay,[1] Nathalie Dereuddre-Bosquet,[2] Judith A. Burger,[3] Meliawati Poniman,[3] Marloes Grobben,[3] Marlyse Buisson,[1] Sebastian Dergan Dylon,[1] Thibaut Naninck,[2] Julien Lemaitre,[2] Wesley Gros,[2] Anne-Sophie Gallouët,[2] Romain Marlin,[2] Camille Bouillier,[2] Vanessa Contreras,[2] Francis Relouzat,[2] Daphna Fenel,[1] Michel Thepaut,[1] Isabelle Bally,[1] Nicole Thielens,[1] Franck Fieschi,[1] Guy Schoehn,[1] Sylvie van der Werf,[4,5] Marit J. van Gils,[3] Rogier W. Sanders,[3,6] Pascal Poignard,[1] Roger Le Grand,[2,*] and Winfried Weissenhorn[1,8,*]

[1]Univ. Grenoble Alpes, CEA, CNRS, Institut de Biologie Structurale (IBS), Grenoble, France
[2]Center for Immunology of Viral, Auto-immune, Hematological and Bacterial Diseases (IMVA-HB/IDMIT), Université Paris-Saclay, Inserm, CEA, Fontenay-aux-Roses, France
[3]Department of Medical Microbiology and Infection Prevention, Amsterdam University Medical Centers, University of Amsterdam, Location AMC, Amsterdam, the Netherlands
[4]Molecular Genetics of RNA Viruses, Department of Virology, Institut Pasteur, CNRS UMR 3569, Université de Paris, Paris, France
[5]National Reference Center for Respiratory Viruses, Institut Pasteur, Paris, France
[6]Department of Microbiology and Immunology, Weill Medical College of Cornell University, New York, NY, USA
[7]These authors contributed equally
[8]Lead contact
*Correspondence: winfried.weissenhorn@ibs.fr (W.W.), roger.le-grand@cea.fr (R.L.G.)
https://doi.org/10.1016/j.xcrm.2022.100528

SUMMARY

The severe acute respiratory syndrome coronavirus 2 (SARS-CoV-2) pandemic has caused an ongoing global health crisis. Here, we present as a vaccine candidate synthetic SARS-CoV-2 spike (S) glycoprotein-coated lipid vesicles that resemble virus-like particles. Soluble S glycoprotein trimer stabilization by formaldehyde cross-linking introduces two major inter-protomer cross-links that keep all receptor-binding domains in the "down" conformation. Immunization of cynomolgus macaques with S coated onto lipid vesicles (S-LVs) induces high antibody titers with potent neutralizing activity against the vaccine strain, Alpha, Beta, and Gamma variants as well as T helper (Th)1 $CD4^+$-biased T cell responses. Although anti-receptor-binding domain (RBD)-specific antibody responses are initially predominant, the third immunization boosts significant non-RBD antibody titers. Challenging vaccinated animals with SARS-CoV-2 shows a complete protection through sterilizing immunity, which correlates with the presence of nasopharyngeal anti-S immunoglobulin G (IgG) and IgA titers. Thus, the S-LV approach is an efficient and safe vaccine candidate based on a proven classical approach for further development and clinical testing.

INTRODUCTION

Severe acute respiratory syndrome coronavirus 2 (SARS-CoV-2), a betacoronavirus closely related to SARS-CoV-1, is the etiological agent of coronavirus disease (COVID-19), which quickly developed into a worldwide pandemic[1,2] causing more than five million deaths as of November 2021 (https://covid19.who.int/) and highlighting the urgent need for effective infection control and prevention.

An important correlate of protection of antiviral vaccines is the generation of neutralizing antibodies.[3–5] The main SARS-CoV-2 target for inducing neutralizing antibodies is the spike (S) glycoprotein composed of the S1 subunit that harbors the receptor-binding domain (RBD) and the S2 membrane fusion subunit that anchors the S trimer in the virus membrane.[6] RBD binding to the cellular receptor ACE 2 (ACE2) leads to virus attachment, and subsequent S2-mediated fusion with endosomal membranes establishes infection.[7–9] S is synthesized as a trimeric precursor polyprotein that is proteolytically cleaved by furin and furin-like proteases in the Golgi generating the non-covalently linked S1-S2 heterotrimer.[10] The structure of S reveals a compact heterotrimer composed of the S1 N-terminal domain (NTD), the receptor-binding domain (RBD) , two subdomains, S2, the transmembrane region, and a cytoplasmic domain. The conformation of RBD is in a dynamic equilibrium between either all RBDs in a closed, receptor-inaccessible conformation or one or two RBDs in the "up" conformation.[8,11–14] Only the S RBD in the up position allows receptor binding,[15,16] which triggers the

S2 post-fusion conformation in proteolytically cleaved S.[14] S is also highly glycosylated, which affects infection[17] and access to neutralizing antibodies.[18]

Antibodies targeting the S glycoprotein were identified upon SARS-CoV-2 seroconversion,[19] which mostly target RBD that is immunodominant.[20,21] This led to the isolation of many neutralizing antibodies, which confirmed antibody-based vaccination strategies.[22–36] Many of these antibodies have been shown to provide *in vivo* protection against SARS-CoV-2 challenge in small animals and non-human primates[28,36–39] or are in clinical development and use.[40]

The magnitude of antibody responses to S during natural infection varies greatly and correlates with disease severity and duration.[41,42] Basal responses are generally maintained for months[43–45] or decline within weeks after infection,[41] most notably in asymptomatic individuals.[46] Thus, any vaccine-based approach aims to induce long-lasting immunity.

A number of animal models have been developed to study SARS-CoV-2 infection including the macaque model, which demonstrated an induction of innate, cellular, and humoral responses upon infection,[47–51] conferring partial protection against reinfection.[52,53] Consequently, many early vaccine candidates provided protection in the macaque model including the currently licensed vaccines based on S-specific mRNA delivery[54,55] (BNT162b2, Pfizer/BioNTech; mRNA-1273, Moderna), adenovirus vectors[56,57] (ChAdOx1 nCoV-19, Oxford/AstraZeneca; Ad*26*.COV2.S, Johnson & Johnson), and inactivated SARS-CoV-2[58,59] (PiCoVacc/CoronaVac, Sinovac). Numerous other approaches have been evaluated as well.[60]

Employing the classical subunit approach, S subunit vaccine candidates have generated different levels of neutralizing antibody responses in pre-clinical testing.[61–65] Using self-assembly strategies of S or RBDs further increased immune responses[66,67] and protected against infection.[68–70]

Antigens can be also presented via liposomes, which provide a highly controllable degree of multivalency and stability and a prolonged circulating half-life *in vivo.*[71,72] Notably, liposomes coated with viral glycoproteins such as the HIV-1 envelope (Env) induced more efficient immune responses than did immunization with single glycoprotein trimers.[73–76] This is in line with more efficient B cell activation and with the generation of germinal centers (GCs) by multivalent presentation of Env trimers versus soluble trimers.[73]

Here, we developed synthetic virus-like particles employing liposomes that are decorated with S glycoprotein trimers that have been treated by formaldehyde cross linking, which in turn stabilized S in the native conformation over a long time period. Serum antibody recognition of cross-linked versus non-cross-linked S did not show significant binding differences. A small group of cynomolgus macaques was immunized with S-LVs, which produced high S-specific antibody titers and Th1 $CD4^+$ T cell responses. Potent neutralization of wild-type (WT) SARS-CoV-2 and of Alpha pseudovirus variants was observed after two immunizations, while Beta and Gamma pseudovirus variants were neutralized at reduced potency. Challenge of the animals with SARS-CoV-2 demonstrated that S-LV immunization protected the animals from infection revealing no detection of genomic RNA (gRNA) upon infection in nasal and tracheal swabs nor in bronchoalveolar lavages (BALs), thus suggesting sterilizing immunity. This indicates that S-LVs are potential candidates for further clinical development of a safe protein-based SARS-CoV-2 vaccine.

RESULTS

S-LV formation and characterization

The S glycoprotein construct 2P[8] was expressed in mammalian cells and purified by Ni^{2+}-affinity and size-exclusion chromatography (SEC) (Figure S1A), with yields up to 10 mg/L using Expi293F cells. This produced native trimers as determined by negative staining electron microscopy and 2D class averaging of the single particles (Figure S1B). Since S revealed low thermostability (melting temperature [Tm] = 42°C) as reported previously,[8] it was chemically cross-linked with 4% formaldehyde (FA) producing a higher molecular weight species as determined by SDS-PAGE (Figure S1C). FA cross-linking preserved the native structure (Figure S1D) over longer time periods (Figures S1E) by increasing the thermostability to a Tm of 65°C. The cryo-electron microscopy structure of FA-cross-linked S (FA-S) at 3.4°C resolution (Figure S2; Table S1) revealed two major sites of cross linking (Figure 1A). RBD residues R408 and K378 cross-linked neighboring RBDs producing S trimers in the closed "RBD-down" conformation (Figures 1A and 1B). The second site introduced inter-S2 subunit bonds by cross-linking R1019 of the central S2 helix and/or S2 K776 with S2 HR1 K947 (Figure 1C). FA-S was incubated with liposomes (phosphatidylcholine 60%, cholesterol 36%, DGS-NTA 4%), and efficiently captured via its C-terminal His-tag. Free, unbound Fa-S was removed from the S proteoliposomes by sucrose gradient centrifugation (Figure S1F), and decoration of the liposomes with FA-S (S-LV) was confirmed by negative staining electron microscopy (Figure 1D).

S-LV immunization induced potent neutralizing antibody responses in cynomolgus macaques

S-LVs were produced for a small vaccination study of cynomolgus macaques to evaluate the immunogenicity and elicitation of neutralizing antibodies. Four cynomolgus macaques were immunized with 50 μg S-LVs adjuvanted with monophospholipid A (MPLA) liposomes by the intra-muscular route at weeks 0, 4, 8, and 19 (Figure 2A). Sera of the immunized macaques were analyzed for binding to S, FA-S, and the RBD in 2 week intervals. The results revealed similar S-specific antibody (Ab) titers for all animals. S effective dose (ED_{50}) titers increased from ∼75 on week 4 to ∼10,000 on week 6 and to ∼20,000 on week 12, after the first, second, and third immunizations, respectively (Figure 2B). Slight reductions in titers were detected against FA-S (Figure 2C). Titers against RBD alone reached effective doses (ID50s) of ∼100 on week 4 and ∼4,500 on week 6, as well as slight increases on week 12 for some animals (Figure 2D). This suggests that the first and second immunizations induced significant RBD titers, while the third immunization boosted non-RBD antibodies since the week 12 S-specific titers were >4 times higher than the RBD-specific titers in contrast to previous time points at which this ratio was lower (Figure 2C). A fourth immunization did not further boost antibody generation, and titers at week 22 were lower or comparable to week 12 titers (Figures

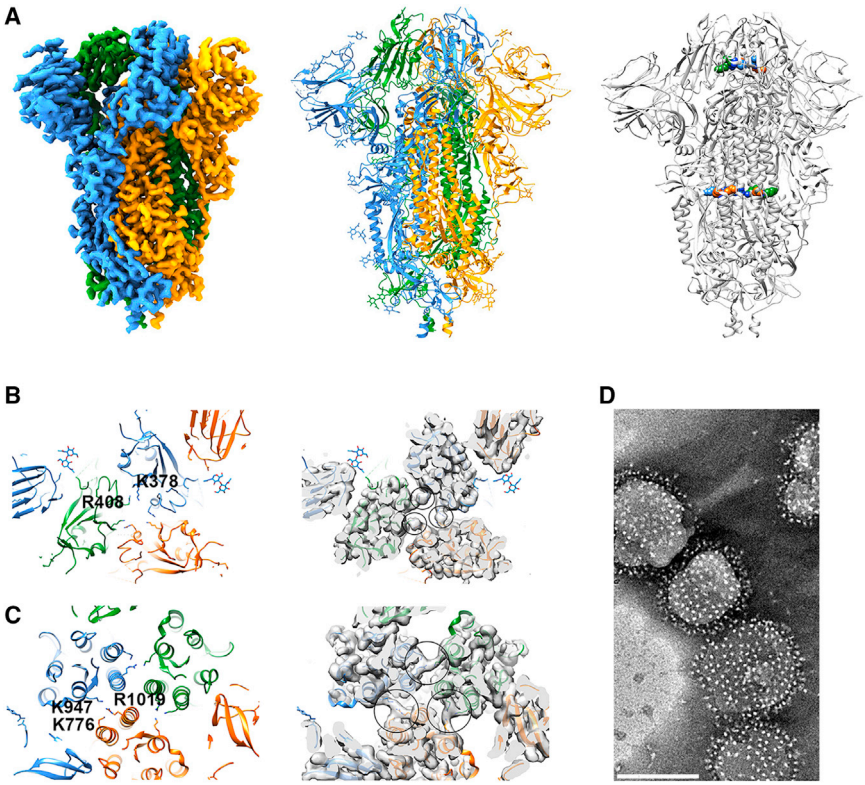

Figure 1. Structural characterization of cross-linked SARS-CoV-2 S (FA-S)- and FA-S-coated lipid vesicles (LVs)

(A) Right panel, cryo-EM density of FA-S with all three RBDs down; each protomer is colored differently. The structure was calculated from 126,719 particles imposing C3 symmetry. . Middle panel, molecular model of FA-S refined to a resolution of 3.4 Å shown as ribbon. Modeled *N*-linked glycans are shown as all atom models. Right panel, two major cross-linking sites were identified that covalently link RBDs and the S2 subunits from different protomers.

(B) Close-up of the cross-linking sites between RBDs. FA-cross-linked amino groups of K378 and R408 of neighboring protomers as indicated by the continuous density connecting side chains (right panel).

(C) Close-up of the cross-linking sites between S2 (left panel). Continuous density between the central helix R1019 as well as S2 K776 to S2 HR1K947 suggested two alternative cross-links between protomers with equal occupancy (right panel).

(D) FA-cross-linked S glycoprotein was incubated with liposomes containing 4% DGS-NTA lipids, purified by sucrose gradient density centrifugation, and analyzed by negative staining electron microscopy, revealing regular decoration of the liposomes with the S glycoprotein. Counting S on 50 S-LVs (negative staining EM 2D vision) indicated 231 ± 92 trimers. We thus estimate that approximately or at least 460 ± 184 S trimers are attached to the LVs. Scale bar, 200 nm.

2B, 2C, and 2D). We conclude that S-LV immunization induced primarily RBD-specific antibodies after the first and second immunizations, while the third immunization increased the generation of non-RBD antibodies significantly.

Serum neutralization titers using a WT pseudovirus were elicited in all four animals. At week 2 after the first immunization, ID50 titers between 100 and 1,000 were observed, which dropped close to baseline at week 4 but was significantly increased at week 6, 2 weeks after the second immunization demonstrating ID50s between 5,000 and ~20,000. The ID50s then decreased at week 8 and increased from 20,000 to ~40,000 at week 10, 3 weeks after the third immunization. At week 19, neutralization potency decreased but was still high, indicating that three immunizations induced robust neutralization titers. The fourth immunization boosted neutralization titers to the same level as the third immunization (Figure 3A).

Since antibody titers indicated the induction of high levels of RBD-specific antibodies, in order to understand the part of anti-RBD antibodies in serum neutralization, we depleted the serum at week 10 by anti-RBD affinity chromatography, resulting in no detectable RBD antibodies by ELISA. RBD-specific Ab-depleted serum showed 10% to 30% neutralization compared with the complete serum, indicating some level of non-RBD-specific neutralization. While RBD-specific Ab neutralization largely dominated in two animals, the fraction of non-RBD-specific Ab neutralization activity (Figure 3B) appeared greater in the other two, suggesting a participation of these Abs in the high neutralization titers (Figure 3A).

S-LV immunization protected cynomolgus macaques from SARS-CoV-2 infection

In order to determine the extent of S-LV-vaccination-induced protection, vaccinated and non-vaccinated animals (n = 4) were infected with the primary SARS-CoV-2 isolate (BetaCoV/France/IDF/0372/2020) with a total dose of 1×10^5 plaque-forming units (PFU). Infection was induced by combining intra-nasal (0.25 mL into each nostril) and intra-tracheal (4.5 mL) routes at week 24, 5 weeks after the last immunization. Viral loads in the control animal group peaked in the trachea at 3 days post-exposure (dpe) with a median value of 6.0 $\log_{10}$ copies/mL and in the nasopharynx between 4 and 6 dpe with a median copy number of 6.6 $\log_{10}$ copies/mL (Figure 4A). Viral loads decreased subsequently, and no virus was detected on 10 dpe in the trachea, while some animals showed viral detection up to 14 dpe in the nasopharyngeal swabs (Figure 4A). In the BAL, three control (Ctrl) animals out of four showed detectable viral loads at 3 dpe, and two of them remained detectable at 7 dpe with mean value of 5.4 and 3.6 $\log_{10}$ copies/mL, respectively. Rectal fluids tested positive in one animal, which also had the highest tracheal and nasopharyngeal viral loads (Figures S3A and S3B). Viral subgenomic RNA (sgRNA), which is believed to estimate the number of infected and productively infected cells collected with the swabs or during the lavage, showed peak copy numbers between 3/4 and 6 dpe in the tracheal and nasopharyngeal fluids, respectively (Figure 4B). In the BALs, the two animals presenting high genomic viral loads also showed detectable sgRNA at 3 and 7 dpe, with medians of 5.1 and 3.1 $\log_{10}$ copies/mL, respectively (Figure 4B).

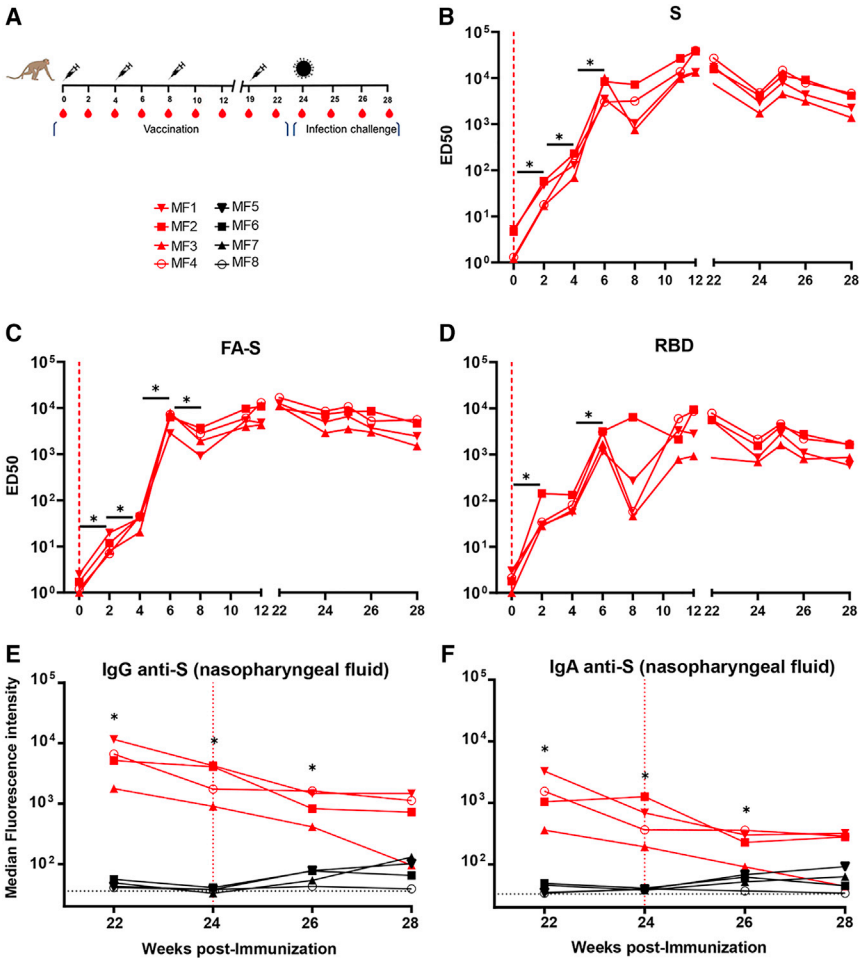

Figure 2. Antibody responses induced by S-LV vaccination of cynomolgus macaques

(A) Scheme of vaccination, challenge, and sampling. Syringes indicate the time points of vaccination, red drops indicate the time of serum collection, and the virus particle indicates the time point of challenge. Symbols of identifying individual macaques are used in all figures.

(B) ELISA of SARS-CoV-2 S-protein-specific IgG determined during the study at weeks 0, 2, 4, 6, 8, 10, 12, 22, 24, 26, and 28. Ab titers of individual animals are shown.

(C) ELISA of SARS-CoV-2 FA-S-protein-specific IgG determined during the study at the indicated weeks.

(D) ELISA of SARS-CoV-2 S RBD-specific IgG determined during the study at the indicated weeks.

(B–D) Differences between matched groups were compared using the Wilcoxon signed-rank test ($p < 0.1$).

(E and F) Detection of S-specific IgG (E) and IgA (F) in nasopharyngeal fluids. Relative mean fluorescence intensity (MFI) of IgG and IgA binding to SARS-CoV-2 S measured with a Luminex-based serology assay in nasopharyngeal swabs. The background level is indicated by dotted lines. The vertical red line indicates the day of challenge. Groups were compared using the Mann-Whitney U test (*$p < 0.05$).

Data presented are from technical duplicates.

In contrast to control animals, neither gRNA nor sgRNA was detected at any point in the vaccinated group (Figures 4A and 4B). The mean gRNA peaks in the trachea and nasopharynx (6.0 and 6.6 $\log_{10}$ copies/mL, respectively) of the control group were higher ($p = 0.0286$) than those of the vaccinated group. The area under the curve was also higher in the trachea of the control group (6.2 $\log_{10}$, $p = 0.286$). In the BAL, the difference was not statistically significant due to the low number of animals. The complete absence of viral RNA in the vaccinated group, both in the upper and lower respiratory tract, strongly suggested that sterilizing immunity was induced by vaccination. ID50 antibody titers against S, FA-S, and the RBD decreased slightly from the day of infection (week 24) to 4 weeks pe (Figures 5A, 5B, and5C), although a small increase in Ab titers is observed at 1 week pe (week 25). Ab titers also correlated with a slight decrease in neutralization from week 24 to 4 weeks pe, although one animal showed a small increase in neutralization on week 25, 1 week pe (Figure 5D). This demonstrated that challenge of vaccinated animals did not significantly boost their immune system. In contrast, the control group started to show clear detection of S-, FA-S-, and RBD-specific IgG on week 2 pe (week 26) (Figures 5A, 5B, and 5C), which correlated with the detection of neutralization at week 2 pe in most animals (Figure 5D). Protection of vaccinated animals further correlated with the presence of significant S- and RBD-specific IgG and IgA in nasopharyngeal fluids (Figures 2E and S4). This indicated that S-LV vaccination induced mucosal immunity that very likely contributed to the sterilizing effect of vaccination.

Similar to previous observations,[50,70] during the first 14 dpe, all control animals showed mild pulmonary lesions characterized by non-extended ground-glass opacities (GGOs) detected by chest CT (Figure S5A). Vaccinated animals showed no significant impact of challenge on CT scores. The only animal showing a lesion score >10 was in the control group. Whereas all control animals experienced monocytoses between 2 and 8 dpe, probably corresponding to a response to infection, monocyte counts remained stable after challenge for the vaccinated monkeys (Figure S5B), in agreement with the absence of detectable anamnestic response in the latter animals.

The levels of CD4- and CD8-specific T cells were measured in both groups of animals. Before exposure, Th1-type $CD4^+$ T cell responses were observed in all vaccinated macaques following *ex vivo* stimulation of peripheral blood mononuclear cells (PBMCs) with S-peptide pools (Figures 6, S6, and S7). None had detectable anti-S $CD8^+$ T cells (Figure S8). No significant difference was observed at 14 dpe, also in agreement with the absence of an anamnestic response in vaccinated animals. In contrast, the anti-S Th1 $CD4^+$ response increased post-exposure for most of the control animals (Figures 6 and S6).

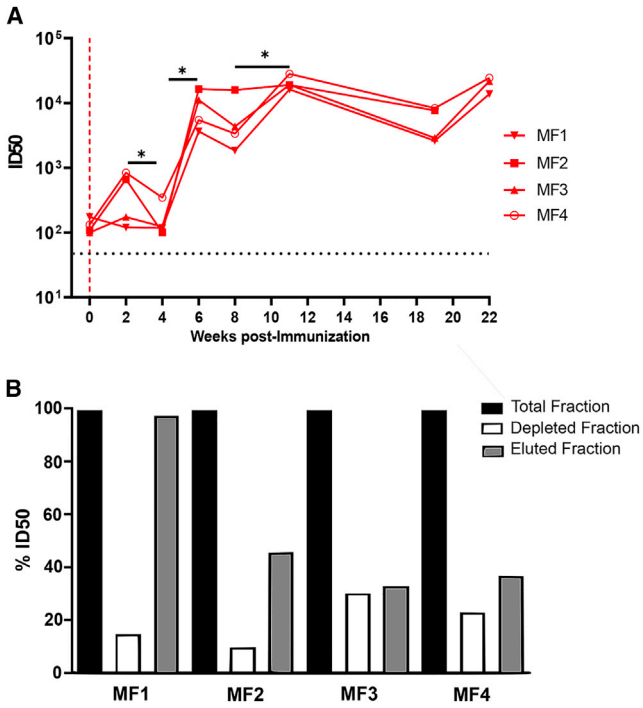

Figure 3. Serum neutralization of SARS-CoV-2 pseudovirus upon S-LV vaccination

(A) The evolution of SARS-CoV-2 neutralizing Ab titers is shown for sera collected at weeks 0, 2, 4, 6, 8, 10, 12, and 19. Bars indicate median titers of the four animals. Differences between matched groups were compared using the Wilcoxon signed-rank test ($p < 0.1$). Data presented are from technical duplicates.

(B) Serum from week 10 was depleted of RBD-specific Abs by affinity chromatography, and neutralization activity of the complete serum of each animal was set to 100% and compared with the RBD-depleted sera and the RBD-specific sera.

We conclude that S-LV vaccination can produce sterilizing immunity, indicating that such a vaccination scheme would be efficient to interrupt the chain of SARS-CoV-2 transmission.

S-LV vaccination generated robust neutralization of SARS-CoV-2 variants

Serum neutralization was further tested against variants B.1.1.7 (Alpha, UK), B.1.351 (Beta, South Africa [SA]), and P.1 (Gamma, Brazil [BR]). Comparing the sera of the vaccinated and non-vaccinated groups at weeks 24 and 28 showed high neutralization titers for all three variants, with median ID50s ranging from 10,000 to 20,000, comparable to WT pseudovirus neutralization (Figure S9). However, since the background of pre-exposure serum neutralization of the non-vaccinated challenge group was relatively high (median ID50s ranging from 400 to 1,100), we repeated the neutralization with purified IgG from serum samples of the vaccinated group from week 8 (after two immunizations), week 12 (3 immunizations) and weeks 24 and 28 (4 immunizations). This showed median ID50s of ~4,500 for WT and Alpha on week 8 (Figure 7), comparable to WT serum neutralization (Figure 3A). Lower ID50s were observed against Beta and Gamma at week 8. Neutralization potency was increased after the third immunization (week 12), with median ID50s of ~5,000 (WT), ~8,000 (Alpha), ~800 (Beta), and 1,000 (Gamma). Neutralization titers did not increase after the fourth immunization at week 24 and started to decrease at week 28 (Figure 7). We conclude that three immunizations provided robust protection against the variants, although neutralization titers may have already been within the protective range after two immunizations for the three variants tested.

DISCUSSION

Many vaccines are under development in pre-clinical and clinical testing,[60] and eight have been approved by regulatory agencies around the world. Here, we developed a two-component system employing the SARS-CoV-2 S glycoprotein coupled to liposomes. Since the stability of the WT SARS-CoV-2 S glycoprotein is low due to its tendency to spontaneously switch into its post-fusion conformation,[14] SARS-CoV-2 S was stabilized by two proline mutations that enhanced stability.[8] However, this S 2P version still showed limited stability over time, as reported,[8] which may be due to cold sensitivity.[77] We overcame the problem of stability by using FA cross-linking that increased the thermostability to 65°C, preserving the native S conformation over extended storage time periods. Furthermore, we detected two cross-linking sites by cryoelectron microscopy (cryo-EM), which showed that cross-linking locked the native S trimer in the closed, RBD-down conformation via covalent inter-protomer interactions, which prevent conformational changes leading to the post-fusion conformation. Notably, FA cross-linking is widely used in vaccine formulations.[78] S stability has since been improved by engineering six proline mutations (S 6P), which increased the thermostability to 50°C,[79] and by disulfide-bond engineering.[80] Moreover, ligand binding renders S more stable.[81,82]

Many previous studies have shown that immunogen multimerization strategies are highly beneficial for B cell activation, including the use of synthetic liposomes[71,72] such as HIV-1 Env-decorated liposome vaccination strategies.[76] We linked SARS-CoV-2 S to liposomes producing synthetic virus-like particles with controlled diameters. Our data show that the S-LVs show similar immunogenic properties as a number of reported self-assembling particles of SARS-CoV-2 RBDs and S.[66,67,69,70,83,84] Our S-LVs induce robust and potent neutralizing responses in cynomolgus macaques, which completely protected the animals from infection by sterilizing immunity. Notably, no signs of virus replication could be detected in the upper and lower respiratory tracts, consistent with the absence of clinical signs of infection such as lymphopenia and lung damage characteristics for COVID-19. The important correlate of protection against SARS-CoV-2 is provided by neutralizing antibodies.[51,85,86] The S-LV approach induces high titers already after two immunizations, with a median ID50 of ~8,000 2 weeks after the second immunization, which is substantially higher than neutralizing Ab responses reported for vaccines tested in non-human primate (NHP) studies, including licensed ones. Adenovirus-based vaccines (AstraZeneca ChAdOx1; Janssen AD26COV2SPP°),[56,57] inactivated virus vaccines (Sinovac PiCoVacc; Sinopharm/BIBP BBIP-CorV),[58,59] a DNA vaccine,[85]

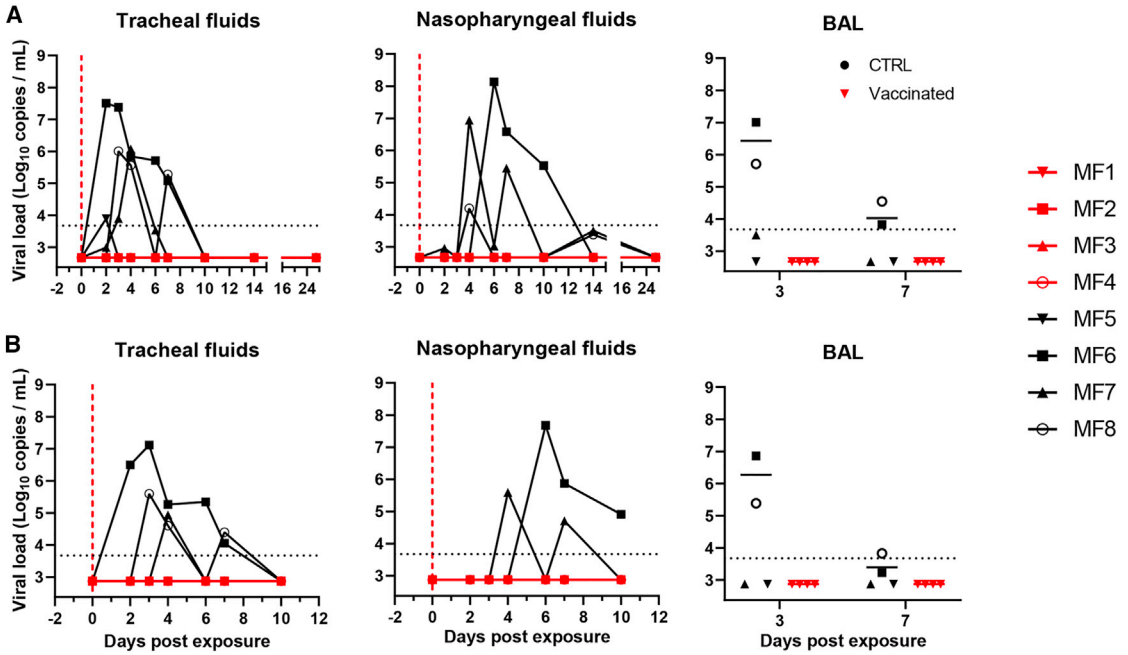

Figure 4. S-LV immunization protects cynomolgus macaques from SARS-CoV-2 infection

Genomic (A) and subgenomic (sg)RNA viral loads (B) in tracheal swabs (left) and nasopharyngeal swabs (middle) of control (black) and vaccinated (red) macaques after challenge. Viral loads in control and vaccinated macaques after challenge in BAL are shown (right). Bars indicate median viral loads. Vertical red dotted lines indicate the day of challenge. Horizontal dotted lines indicate the limit of quantification. Data presented are from technical duplicates.

and an mRNA vaccine (Pfizer/BionTech BNT162b2)[55] showed 10–20 times lower titers compared with the S-LVs in macaques studies. Further, the Moderna mRNA-1273 (Moderna),[54] S trimers (Clover Biopharmaceutical),[64] and NVX-CoV2373 (Novavax)[69] induced similar or higher titers in macaque studies. Median ID50 titers increased by a factor of ~4 after the third immunization but did not amplify after the fourth immunization. The T cell response in the vaccinated group was biased toward Th1 $CD4^+$ T cells, consistent with licensed or other experimental vaccines.[54,87–90]

Serum neutralization was already significant after the first immunization but increased by a factor of ~20 after the second immunization and by a factor of 3 after the third immunization, indicating that two immunizations with S-LVs may suffice to confer protection. Neutralizing antibody (nAb) titers decline within 10 weeks after the third immunization to the levels of week 8

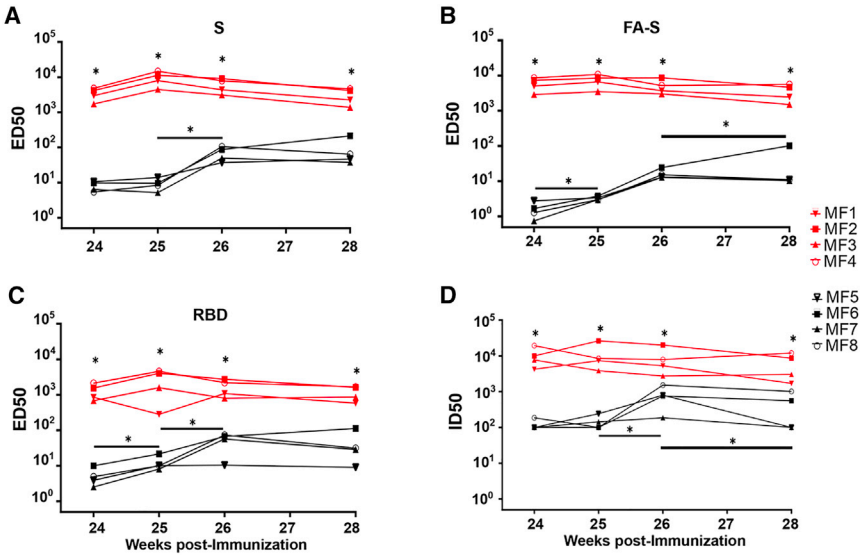

Figure 5. Serum antibody titers and neutralization of vaccinated and control group cynomolgus macaques after SARS-CoV-2 challenge

(A–C) Antibody IgG titers were determined by ELISA at weeks 24 (challenge), 25, 26, 27, and 28 against (A) SARS-CoV-2 S, (B) SARS-CoV-2 FA-S, and (C) SARS-CoV-2 S RBD. Vaccinated animals are shown with red symbols and control animals with black symbols.

(D) SARS-CoV-2 pseudovirus neutralization titers at week 24 (challenge) and 1, 2, and 4 weeks post-exposure (weeks 25, 26, and 28). The bars show the median titers.

Differences between matched groups were compared using the Wilcoxon signed-rank test ($p < 0.1$). Neutralization data presented are from technical triplicates.

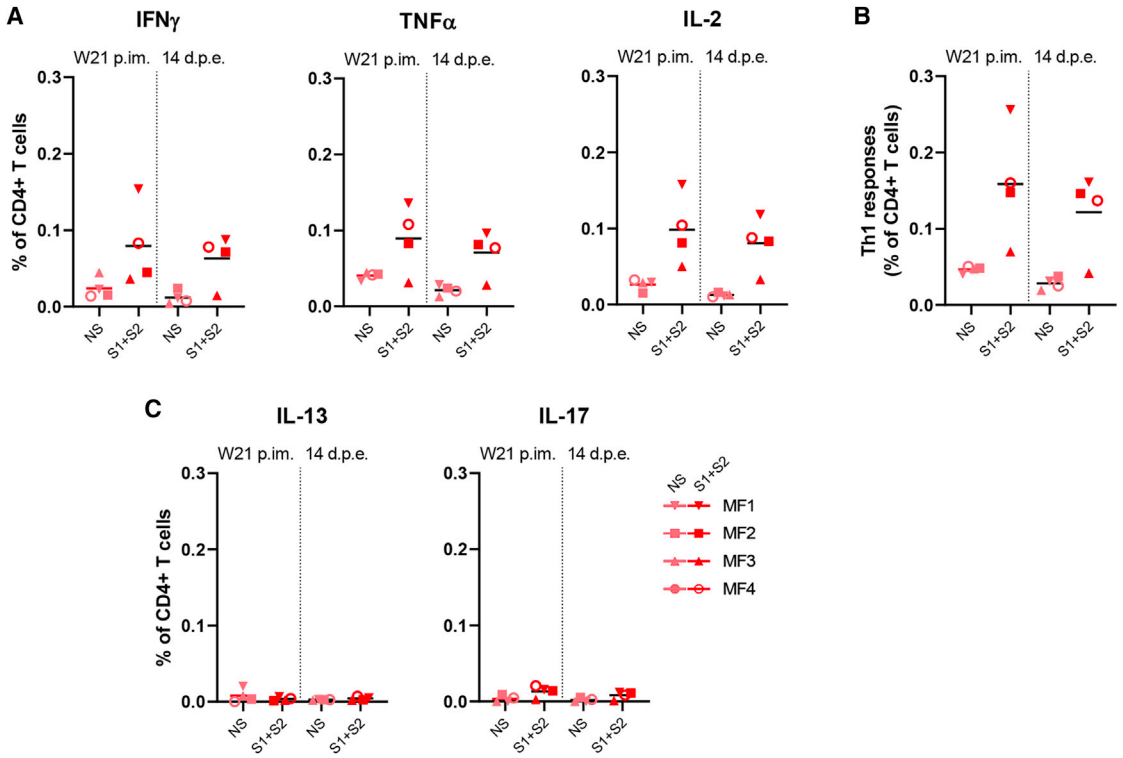

Figure 6. Antigen-specific CD4 T cell responses in S-LV-immunized cynomolgus macaques

Frequency of (A) interferon gamma (IFNγ)+, tumor necrosis factor alpha (TFNα)+, and interleukin (IL)-2+, (B) Th1 (IFNγ+/–, IL-2+/–, TNFα+), and (C) IL-13+ and IL-17+ antigen-specific $CD4^+$ T cells (CD154+) in the total $CD4^+$ T cell population, respectively, for each immunized macaque (n = 4) at week 21 (W21) post-immunization (p.im.) (i.e., 2 weeks after the fourth immunization, pre-exposure) and 14 days post-exposure (dpe). PBMCs were stimulated overnight with medium (pink symbols) or SARS-CoV-2 S overlapping peptide pools (red symbols). Bars indicate means. Time points in each experimental group were compared using the Wilcoxon signed rank test.

(prior to the third immunization) and increase slightly after the fourth immunization to the median ID50 level attained after the third immunization.

Vaccination prevented lymphopenia and lung damage in animals infected with SARS-CoV-2 at a dose comparable[54,56,57,69,85] or lower[70] than in previous studies. Protection was sterilizing since no replication could be detected in the upper and lower respiratory tracts, suggesting that vaccination with S-LVs will prevent virus shedding and transmission. Sterilizing immunity likely correlates with mucosal antibody responses that protect the upper respiratory tract from infection.[43,91] Since we detected significant IgG and IgA in nasopharyngeal fluids at the time of viral challenge, we propose that S-LV vaccination induces sterilizing protection by eliciting mucosal immune responses.

SARS-CoV-2 infection generates nAbs, with up to 90% targeting the RBD, which is immunodominant.[20,33,92] Similarly, mRNA vaccination elicits predominately RBD-specific nAbs.[93] RBD antibodies can be grouped into three classes[94,95] and seem to be easily induced by immunization, as many of them are generated by a few cycles of affinity maturation, indicating that extensive GC reactions are not required.[96] Consistent with these findings, we show that RBD-specific antibodies are predominant after the first and second immunizations as indicated by similar S- and RBD-specific titers. However, after the third immunization, median S-specific ED50s are 3 times higher than RBD-specific ED50s 4 weeks after the third immunization. This trend is continued after the fourth immunization, which revealed a 3.5 times higher median ID50 for S than for RBD 5 weeks post-immunization. This thus suggests that more than two immunizations expand the reactive B cell repertoire that targets non-RBD S epitopes.

Current variants carry the B.1D614G mutation and have been reported to be more infectious.[97–103] Although the D614G mutation alone was reported to increase neutralization susceptibility,[104] further mutations present in Beta (B1.351, SA) and Gamma (P1, BR) reduce neutralization potencies of natural and vaccine-induced sera,[105–112] while Alpha (B.1.1.7, UK) neutralization seems to be less affected.[113] The reduction in neutralization potency of polyclonal plasma Abs is mainly affected by mutations within the three main epitopes in the RBD. In particular, the E484K mutation present in Beta and Gamma was reported to reduce neutralization by a factor of 10.[114] Here, we show that S-LV vaccination produces robust neutralization of Alpha, Beta, and Gamma, although the median ID50s of Beta and Gamma neutralization are reduced 20- and 5-fold, respectively, after the second immunization compared with WT and Alpha. The third immunization boosted neutralization of Beta and Gamma, albeit with 6- and 3-fold reductions in potency,

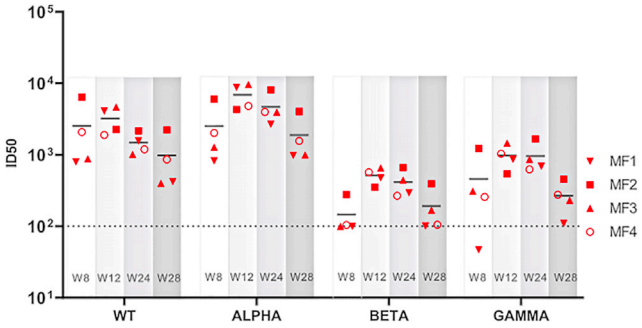

Figure 7. S-vaccination induces robust neutralization of SARS-CoV-2 variants

B.1.1.7 (Alpha, UK), B.1.351 (Beta, SA), and P.1 (Gamma, BR) pseudovirus neutralization titers were compared with the Wuhan vaccine strain. Titers were determined using total IgG purified from sera at weeks 8 (2 immunizations), 12 (3 immunizations), and 24 and 28 (4 immunizations). Background neutralization by IgG isolated from naive animals was <100 for all variants and is indicated by the dashed line. Data presented are from technical triplicates.

respectively, compared with WT, which is slightly more potent than the median ID50 of vaccinated and hospitalized patient cohorts using the same assay setup.[115]

In summary, S-LV vaccination represents an efficient strategy that protects macaques from high-dose challenge. Although the animals have been challenged only after the fourth immunization, which did not boost Ab or neutralization titers significantly, our neutralization data suggest that the animals might have been protected after two immunizations. Furthermore, our data suggest that the third immunization increases S-protein Ab titers more significantly than RBD-specific Ab titers. This points to an increase of non-RBD antibodies, which may be beneficial for the neutralization of different variants. Although other regions within S, most notably NTD, are targets for mutation within new variants, S2 or other epitopes may be less prone to mutations due to conformational constraints. Therefore, future vaccination strategies should consider boosting non-RBD antibodies to compensate for the loss of neutralization activity targeting RBD in variants. Notably, SARS-CoV-2 memory B cells are present over a long time period in convalescent[116,117] and mRNA-vaccinated individuals,[118] which is in line with potential boosting strategies.

Limitations of study

We provide data that the immunization of macaques with synthetic S-glycoprotein-coated liposomes induced robust antibody and neutralization titers after two immunizations. SARS-CoV-2 challenge after four immunizations revealed complete protection by sterilizing immunity. First, a limitation of the study is that the challenge was performed only after the fourth immunization. Secondly, although the SARS-CoV-2 challenge infection was performed 5 weeks after the last immunization, we cannot predict the efficacy of protection months post-immunization. The third limitation of the study is the small number of animals used, which prevents robust statistical analyses of the results. Fourth, although we observe robust pseudovirus neutralization of Alpha, Beta, and Gamma variants, we cannot predict the efficacy of protection upon infection, which will require further studies.

STAR★METHODS

Detailed methods are provided in the online version of this paper and include the following:

- KEY RESOURCES TABLE
- RESOURCE AVAILABILITY
  - Lead contact
  - Materials availability
  - Data and code availability
- EXPERIMENTAL MODEL AND SUBJECT DETAILS
  - Cell lines
  - Viruses
  - Ethics and biosafety statement
  - Animals and study design
- METHODS DETAILS
  - Protein expression and purification
  - SARS-CoV-2 S crosslinking
  - S protein coupling to liposomes
  - S protein thermostability
  - Negative stain electron microscopy
  - Cryo-electron microscopy
  - Virus quantification in NHP samples
  - Chest CT and image analysis
  - ELISA
  - Protein coupling to luminex beads
  - Luminex assay
  - Pseudovirus neutralization assay
  - Antigen specific T cell assays using non-human primate cells
  - Statistical analysis

SUPPLEMENTAL INFORMATION

Supplemental information can be found online at https://doi.org/10.1016/j.xcrm.2022.100528.

ACKNOWLEDGMENTS

This work acknowledges support by the European Union's Horizon 2020 research and innovation program under grant agreement no. 681032, H2020 EHVA (W.W.), the ANR, RA-Covid-19 (W.W. and R.I.G.), and the CNRS (W.W.). W.W. acknowledges access to the platforms of the Grenoble Instruct-ERIC center (IBS and ISBG; UMS 3518 CNRS-CEA-UGA-EMBL) within the Grenoble Partnership for Structural Biology (PSB), with support from FRISBI (ANR-10-INBS-05-02) and GRAL, a project of the University Grenoble Alpes graduate school (Ecoles Universitaires de Recherche) CBH-EUR-GS (ANR-17-EURE-0003). The IBS acknowledges integration into the Interdisciplinary Research Institute of Grenoble (IRIG, CEA) and financial support from CEA, CNRS, and UGA. The Infectious Disease Models and Innovative Therapies (IDMIT) research infrastructure is supported by the Program Investissements d'Avenir, managed by the National Research Agency (ANR) under reference ANR-11-INBS-0008. The Fondation Bettencourt Schueller and the Region Ile-de-France contributed to the implementation of IDMIT's facilities and imaging technologies. The NHP study received financial support from REACTing, the Fondation pour la Recherche Médicale (AM-CoV-Path), and the European Infrastructure TRANSVAC2 (730964). We acknowledge support from CoVIC, supported by the Bill and Melinda Gates Foundation. The virus stock was obtained through the EVAg platform (https://www.european-virus-archive.com/), funded by H2020 (653316). The funders had no role in study design, data collection, data analysis, data interpretation, or data reporting.

We thank J. McLellan for providing the S expression vector; B. Delache, E. Burban, J. Demilly, N. Dhooge, S. Langlois, P. Le Calvez, Q. Sconosciuti, V. Magneron, M. Rimlinger, A. Berriche, J.H. Qiu, M. Potier, J.M. Robert, and C. Dodan for help with animal studies and R. Ho Tsong Fang for his supervision; L. Bossevot, M. Leonec, L. Moenne-Loccoz, and J. Morin for the qRT-PCR and preparation of reagents; M. Gomez-Pacheco and J. van Wassenhove for cellular assays; N. Kahlaoui, B. Fert, and C. Mayet for help with the CT scans and C. Chapon for her supervision; M. Barendji, J. Dinh, and E. Guyon for the NHP sample processing; S. Keyser for the transports organization; F. Ducancel and Y. Gorin for their help with the logistics and safety management; and I. Mangeot for her help with resource management. We thank Antoine Nougairede for sharing the plasmid used for the sgRNA assay standardization. Finally, we thank Dietmar Katinger and Philipp Mundsperger (Polymun) for providing MPLA liposomes. Images in Figures 2A and S1F and the graphical abstract were created with BioRender.com.

AUTHOR CONTRIBUTIONS

Conceptualization, W.W., G.S., R.L.G., and P.M.; funding acquisition, W.W., R.L.G., and R.W.S.; investigation, G.S., P.M., A.A., G.E., D.G., J.A.B., M.P., M.G., M.B., S.D.D., T.N., J.L., W.G., A.-S.G., R.M., C.B., V.C., F.R., and D.F.; methodology, G.S., W.W., P.M., M.J.v.G., R.W.S., P.P., and R.L.G.; formal analyses, G.S., P.M., A.A., N.D.-B., S.D.D., T.N., and A.-S.G.; resources, M.T., I.B., N.T., F.F., N.D.-B., and S.v.d.W.; visualization: G.S., P.M., and G.E.; supervision, W.W., R.L.G., N.D.-B., G.S., M.J.v.G., R.W.S, and P.P.; writing – original draft, W.W., P.M., G.S., and R.L.G.; writing – review & editing, all authors.

DECLARATION OF INTERESTS

The authors declare no competing interests.

Received: July 27, 2021
Revised: November 26, 2021
Accepted: January 19, 2022
Published: January 24, 2022

REFERENCES

1. Zhou, P., Yang, X.L., Wang, X.G., Hu, B., Zhang, L., Zhang, W., Si, H.R., Zhu, Y., Li, B., Huang, C.L., et al. (2020). A pneumonia outbreak associated with a new coronavirus of probable bat origin. Nature *579*, 270–273.
2. Coronaviridae Study Group of the International Committee on Taxonomy of, V (2020). The species Severe acute respiratory syndrome-related coronavirus: classifying 2019-nCoV and naming it SARS-CoV-2. Nat. Microbiol. *5*, 536–544.
3. Plotkin, S.A. (2020). Updates on immunologic correlates of vaccine-induced protection. Vaccine *38*, 2250–2257.
4. Khoury, D.S., Cromer, D., Reynaldi, A., Schlub, T.E., Wheatley, A.K., Juno, J.A., Subbarao, K., Kent, S.J., Triccas, J.A., and Davenport, M.P. (2021). Neutralizing antibody levels are highly predictive of immune protection from symptomatic SARS-CoV-2 infection. Nat. Med. *27*, 1205–1211.
5. Earle, K.A., Ambrosino, D.M., Fiore-Gartland, A., Goldblatt, D., Gilbert, P.B., Siber, G.R., Dull, P., and Plotkin, S.A. (2021). Evidence for antibody as a protective correlate for COVID-19 vaccines. Vaccine *39*, 4423–4428.
6. Dagotto, G., Yu, J., and Barouch, D.H. (2020). Approaches and challenges in SARS-CoV-2 vaccine development. Cell Host Microbe *28*, 364–370.
7. Tortorici, M.A., and Veesler, D. (2019). Structural insights into coronavirus entry. Adv. Virus Res. *105*, 93–116.
8. Wrapp, D., Wang, N., Corbett, K.S., Goldsmith, J.A., Hsieh, C.L., Abiona, O., Graham, B.S., and McLellan, J.S. (2020). Cryo-EM structure of the 2019-nCoV spike in the prefusion conformation. Science *367*, 1260–1263.
9. Letko, M., Marzi, A., and Munster, V. (2020). Functional assessment of cell entry and receptor usage for SARS-CoV-2 and other lineage B betacoronaviruses. Nat. Microbiol. *5*, 562–569.
10. Hoffmann, M., Kleine-Weber, H., and Pohlmann, S. (2020). A multibasic cleavage site in the spike protein of SARS-CoV-2 is essential for infection of human lung cells. Mol. Cell *78*, 779–784.
11. Walls, A.C., Park, Y.J., Tortorici, M.A., Wall, A., McGuire, A.T., and Veesler, D. (2020). Structure, function, and antigenicity of the SARS-CoV-2 spike glycoprotein. Cell *181*, 281–292.
12. Ke, Z., Oton, J., Qu, K., Cortese, M., Zila, V., McKeane, L., Nakane, T., Zivanov, J., Neufeldt, C.J., Cerikan, B., et al. (2020). Structures and distributions of SARS-CoV-2 spike proteins on intact virions. Nature *588*, 498–502.
13. Turonova, B., Sikora, M., Schurmann, C., Hagen, W.J.H., Welsch, S., Blanc, F.E.C., von Bulow, S., Gecht, M., Bagola, K., Horner, C., et al. (2020). In situ structural analysis of SARS-CoV-2 spike reveals flexibility mediated by three hinges. Science *370*, 203–208.
14. Cai, Y., Zhang, J., Xiao, T., Peng, H., Sterling, S.M., Walsh, R.M., Jr., Rawson, S., Rits-Volloch, S., and Chen, B. (2020). Distinct conformational states of SARS-CoV-2 spike protein. Science *369*, 1586–1592.
15. Yan, R., Zhang, Y., Li, Y., Xia, L., Guo, Y., and Zhou, Q. (2020). Structural basis for the recognition of SARS-CoV-2 by full-length human ACE2. Science *367*, 1444–1448.
16. Lan, J., Ge, J., Yu, J., Shan, S., Zhou, H., Fan, S., Zhang, Q., Shi, X., Wang, Q., Zhang, L., et al. (2020). Structure of the SARS-CoV-2 spike receptor-binding domain bound to the ACE2 receptor. Nature *581*, 215–220.
17. Thépaut, M., Luczkowiak, J., Vivès, C., Labiod, N., Bally, I., Lasala, F., Grimoire, Y., Fenel, D., Sattin, S., Thielens, N., et al. (2021). DC/L-SIGN recognition of spike glycoprotein promotes SARS-CoV-2 trans-infection and can be inhibited by a glycomimetic antagonist. PLoS Pathog. *17*, e1009576.
18. Watanabe, Y., Allen, J.D., Wrapp, D., McLellan, J.S., and Crispin, M. (2020). Site-specific glycan analysis of the SARS-CoV-2 spike. Science *369*, 330–333.
19. Amanat, F., Stadlbauer, D., Strohmeier, S., Nguyen, T.H.O., Chromikova, V., McMahon, M., Jiang, K., Arunkumar, G.A., Jurczyszak, D., Polanco, J., et al. (2020). A serological assay to detect SARS-CoV-2 seroconversion in humans. Nat. Med. *26*, 1033–1036.
20. Piccoli, L., Park, Y.J., Tortorici, M.A., Czudnochowski, N., Walls, A.C., Beltramello, M., Silacci-Fregni, C., Pinto, D., Rosen, L.E., Bowen, J.E., et al. (2020). Mapping neutralizing and immunodominant sites on the SARS-CoV-2 spike receptor-binding domain by structure-guided high-resolution serology. Cell *183*, 1024–1042.
21. Premkumar, L., Segovia-Chumbez, B., Jadi, R., Martinez, D.R., Raut, R., Markmann, A., Cornaby, C., Bartelt, L., Weiss, S., Park, Y., et al. (2020). The receptor binding domain of the viral spike protein is an immunodominant and highly specific target of antibodies in SARS-CoV-2 patients. Sci. Immunol. *5*, eabc8413.
22. Liu, L., Wang, P., Nair, M.S., Yu, J., Rapp, M., Wang, Q., Luo, Y., Chan, J.F., Sahi, V., Figueroa, A., et al. (2020). Potent neutralizing antibodies against multiple epitopes on SARS-CoV-2 spike. Nature *584*, 450–456.
23. Wec, A.Z., Wrapp, D., Herbert, A.S., Maurer, D.P., Haslwanter, D., Sakharkar, M., Jangra, R.K., Dieterle, M.E., Lilov, A., Huang, D., et al. (2020). Broad neutralization of SARS-related viruses by human monoclonal antibodies. Science *369*, 731–736.
24. Rogers, T.F., Zhao, F., Huang, D., Beutler, N., Burns, A., He, W.T., Limbo, O., Smith, C., Song, G., Woehl, J., et al. (2020). Isolation of potent SARS-CoV-2 neutralizing antibodies and protection from disease in a small animal model. Science *369*, 956–963.
25. Yuan, M., Liu, H., Wu, N.C., Lee, C.D., Zhu, X., Zhao, F., Huang, D., Yu, W., Hua, Y., Tien, H., et al. (2020). Structural basis of a shared antibody response to SARS-CoV-2. Science *369*, 1119–1123.

26. Wang, C., Li, W., Drabek, D., Okba, N.M.A., van Haperen, R., Osterhaus, A., van Kuppeveld, F.J.M., Haagmans, B.L., Grosveld, F., and Bosch, B.J. (2020). A human monoclonal antibody blocking SARS-CoV-2 infection. Nat. Commun. *11*, 2251.

27. Pinto, D., Park, Y.J., Beltramello, M., Walls, A.C., Tortorici, M.A., Bianchi, S., Jaconi, S., Culap, K., Zatta, F., De Marco, A., et al. (2020). Cross-neutralization of SARS-CoV-2 by a human monoclonal SARS-CoV antibody. Nature *583*, 290–295.

28. Zost, S.J., Gilchuk, P., Case, J.B., Binshtein, E., Chen, R.E., Nkolola, J.P., Schafer, A., Reidy, J.X., Trivette, A., Nargi, R.S., et al. (2020). Potently neutralizing and protective human antibodies against SARS-CoV-2. Nature *584*, 443–449.

29. Kreer, C., Zehner, M., Weber, T., Ercanoglu, M.S., Gieselmann, L., Rohde, C., Halwe, S., Korenkov, M., Schommers, P., Vanshylla, K., et al. (2020). Longitudinal isolation of potent near-germline SARS-CoV-2-neutralizing antibodies from COVID-19 patients. Cell *182*, 1663–1673.

30. Baum, A., Ajithdoss, D., Copin, R., Zhou, A., Lanza, K., Negron, N., Ni, M., Wei, Y., Mohammadi, K., Musser, B., et al. (2020). REGN-COV2 antibodies prevent and treat SARS-CoV-2 infection in rhesus macaques and hamsters. Science *370*, 1110–1115.

31. Hansen, J., Baum, A., Pascal, K.E., Russo, V., Giordano, S., Wloga, E., Fulton, B.O., Yan, Y., Koon, K., Patel, K., et al. (2020). Studies in humanized mice and convalescent humans yield a SARS-CoV-2 antibody cocktail. Science *369*, 1010–1014.

32. Brouwer, P.J.M., Caniels, T.G., van der Straten, K., Snitselaar, J.L., Aldon, Y., Bangaru, S., Torres, J.L., Okba, N.M.A., Claireaux, M., Kerster, G., et al. (2020). Potent neutralizing antibodies from COVID-19 patients define multiple targets of vulnerability. Science *369*, 643–650.

33. Robbiani, D.F., Gaebler, C., Muecksch, F., Lorenzi, J.C.C., Wang, Z., Cho, A., Agudelo, M., Barnes, C.O., Gazumyan, A., Finkin, S., et al. (2020). Convergent antibody responses to SARS-CoV-2 in convalescent individuals. Nature *584*, 437–442.

34. Seydoux, E., Homad, L.J., MacCamy, A.J., Parks, K.R., Hurlburt, N.K., Jennewein, M.F., Akins, N.R., Stuart, A.B., Wan, Y.H., Feng, J., et al. (2020). Characterization of neutralizing antibodies from a SARS-CoV-2 infected individual. Immunity *53*, 98–105.

35. Seydoux, E., Homad, L.J., MacCamy, A.J., Parks, K.R., Hurlburt, N.K., Jennewein, M.F., Akins, N.R., Stuart, A.B., Wan, Y.H., Feng, J., et al. (2020). Analysis of a SARS-CoV-2-infected individual reveals development of potent neutralizing antibodies with limited somatic mutation. Immunity *53*, 98–105.

36. Wu, Y., Wang, F., Shen, C., Peng, W., Li, D., Zhao, C., Li, Z., Li, S., Bi, Y., Yang, Y., et al. (2020). A noncompeting pair of human neutralizing antibodies block COVID-19 virus binding to its receptor ACE2. Science *368*, 1274–1278.

37. Tortorici, M.A., Beltramello, M., Lempp, F.A., Pinto, D., Dang, H.V., Rosen, L.E., McCallum, M., Bowen, J., Minola, A., Jaconi, S., et al. (2020). Ultrapotent human antibodies protect against SARS-CoV-2 challenge via multiple mechanisms. Science *370*, 950–957.

38. Hassan, A.O., Case, J.B., Winkler, E.S., Thackray, L.B., Kafai, N.M., Bailey, A.L., McCune, B.T., Fox, J.M., Chen, R.E., Alsoussi, W.B., et al. (2020). A SARS-CoV-2 infection model in mice demonstrates protection by neutralizing antibodies. Cell *182*, 744–753.

39. Alsoussi, W.B., Turner, J.S., Case, J.B., Zhao, H., Schmitz, A.J., Zhou, J.Q., Chen, R.E., Lei, T., Rizk, A.A., McIntire, K.M., et al. (2020). A potently neutralizing antibody protects mice against SARS-CoV-2 infection. J. Immunol. *205*, 915–922.

40. Weinreich, D.M., Sivapalasingam, S., Norton, T., Ali, S., Gao, H., Bhore, R., Musser, B.J., Soo, Y., Rofail, D., Im, J., et al. (2021). REGN-COV2, a neutralizing antibody cocktail, in outpatients with Covid-19. N. Engl. J. Med. *384*, 238–251.

41. Seow, J., Graham, C., Merrick, B., Acors, S., Pickering, S., Steel, K.J.A., Hemmings, O., O'Byrne, A., Kouphou, N., Galao, R.P., et al. (2020). Longitudinal observation and decline of neutralizing antibody responses in the three months following SARS-CoV-2 infection in humans. Nat. Microbiol. *5*, 1598–1607.

42. Chen, Y., Zuiani, A., Fischinger, S., Mullur, J., Atyeo, C., Travers, M., Lelis, F.J.N., Pullen, K.M., Martin, H., Tong, P., et al. (2020). Quick COVID-19 healers sustain anti-SARS-CoV-2 antibody production. Cell *183*, 1496–1507.

43. Isho, B., Abe, K.T., Zuo, M., Jamal, A.J., Rathod, B., Wang, J.H., Li, Z., Chao, G., Rojas, O.L., Bang, Y.M., et al. (2020). Persistence of serum and saliva antibody responses to SARS-CoV-2 spike antigens in COVID-19 patients. Sci. Immunol. *5*, eabe5511.

44. Rodda, L.B., Netland, J., Shehata, L., Pruner, K.B., Morawski, P.A., Thouvenel, C.D., Takehara, K.K., Eggenberger, J., Hemann, E.A., Waterman, H.R., et al. (2021). Functional SARS-CoV-2-specific immune memory persists after mild COVID-19. Cell *184*, 169–183.

45. Iyer, A.S., Jones, F.K., Nodoushani, A., Kelly, M., Becker, M., Slater, D., Mills, R., Teng, E., Kamruzzaman, M., Garcia-Beltran, W.F., et al. (2020). Persistence and decay of human antibody responses to the receptor binding domain of SARS-CoV-2 spike protein in COVID-19 patients. Sci. Immunol *52*, eabe0367.

46. Long, Q.X., Tang, X.J., Shi, Q.L., Li, Q., Deng, H.J., Yuan, J., Hu, J.L., Xu, W., Zhang, Y., Lv, F.J., et al. (2020). Clinical and immunological assessment of asymptomatic SARS-CoV-2 infections. Nat. Med. *26*, 1200–1204.

47. Grifoni, A., Weiskopf, D., Ramirez, S.I., Mateus, J., Dan, J.M., Moderbacher, C.R., Rawlings, S.A., Sutherland, A., Premkumar, L., Jadi, R.S., et al. (2020). Targets of T Cell responses to SARS-CoV-2 coronavirus in humans with COVID-19 disease and unexposed individuals. Cell *181*, 1489–1501.

48. Munster, V.J., Feldmann, F., Williamson, B.N., van Doremalen, N., Perez-Perez, L., Schulz, J., Meade-White, K., Okumura, A., Callison, J., Brumbaugh, B., et al. (2020). Respiratory disease in rhesus macaques inoculated with SARS-CoV-2. Nature *585*, 268–272.

49. Rockx, B., Kuiken, T., Herfst, S., Bestebroer, T., Lamers, M.M., Oude Munnink, B.B., de Meulder, D., van Amerongen, G., van den Brand, J., Okba, N.M.A., et al. (2020). Comparative pathogenesis of COVID-19, MERS, and SARS in a nonhuman primate model. Science *368*, 1012–1015.

50. Maisonnasse, P., Guedj, J., Contreras, V., Behillil, S., Solas, C., Marlin, R., Naninck, T., Pizzorno, A., Lemaitre, J., Goncalves, A., et al. (2020). Hydroxychloroquine use against SARS-CoV-2 infection in non-human primates. Nature *585*, 584–587.

51. McMahan, K., Yu, J., Mercado, N.B., Loos, C., Tostanoski, L.H., Chandrashekar, A., Liu, J., Peter, L., Atyeo, C., Zhu, A., et al. (2021). Correlates of protection against SARS-CoV-2 in rhesus macaques. Nature *590*, 630–634.

52. Deng, W., Bao, L., Liu, J., Xiao, C., Liu, J., Xue, J., Lv, Q., Qi, F., Gao, H., Yu, P., et al. (2020). Primary exposure to SARS-CoV-2 protects against reinfection in rhesus macaques. Science *369*, 818–823.

53. Marlin, R., Godot, V., Cardinaud, S., Galhaut, M., Coleon, S., Zurawski, S., Dereuddre-Bosquet, N., Cavarelli, M., Gallouet, A.S., Maisonnasse, P., et al. (2021). Targeting SARS-CoV-2 receptor-binding domain to cells expressing CD40 improves protection to infection in convalescent macaques. Nat. Commun. *12*, 5215.

54. Corbett, K.S., Flynn, B., Foulds, K.E., Francica, J.R., Boyoglu-Barnum, S., Werner, A.P., Flach, B., O'Connell, S., Bock, K.W., Minai, M., et al. (2020). Evaluation of the mRNA-1273 vaccine against SARS-CoV-2 in nonhuman primates. N. Engl. J. Med. *383*, 1544–1555.

55. Vogel, A.B., Kanevsky, I., Che, Y., Swanson, K.A., Muik, A., Vormehr, M., Kranz, L.M., Walzer, K.C., Hein, S., Guler, A., et al. (2021). BNT162b vaccines protect rhesus macaques from SARS-CoV-2. Nature *592*, 283–289.

56. van Doremalen, N., Lambe, T., Spencer, A., Belij-Rammerstorfer, S., Purushotham, J.N., Port, J.R., Avanzato, V.A., Bushmaker, T., Flaxman, A., Ulaszewska, M., et al. (2020). ChAdOx1 nCoV-19 vaccine prevents SARS-CoV-2 pneumonia in rhesus macaques. Nature *586*, 578–582.

57. Mercado, N.B., Zahn, R., Wegmann, F., Loos, C., Chandrashekar, A., Yu, J., Liu, J., Peter, L., McMahan, K., Tostanoski, L.H., et al. (2020). Single-shot Ad26 vaccine protects against SARS-CoV-2 in rhesus macaques. Nature *586*, 583–588.

58. Gao, Q., Bao, L., Mao, H., Wang, L., Xu, K., Yang, M., Li, Y., Zhu, L., Wang, N., Lv, Z., et al. (2020). Development of an inactivated vaccine candidate for SARS-CoV-2. Science *369*, 77–81.

59. Wang, H., Zhang, Y., Huang, B., Deng, W., Quan, Y., Wang, W., Xu, W., Zhao, Y., Li, N., Zhang, J., et al. (2020). Development of an inactivated vaccine candidate, BBIBP-CorV, with potent protection against SARS-CoV-2. Cell *182*, 713–721.

60. Klasse, P.J., Nixon, D.F., and Moore, J.P. (2021). Immunogenicity of clinically relevant SARS-CoV-2 vaccines in nonhuman primates and humans. Sci. Adv. *7*, eabe8065.

61. Liu, X., Drelich, A., Li, W., Chen, C., Sun, Z., Shi, M., Adams, C., Mellors, J.W., Tseng, C.T., and Dimitrov, D.S. (2020). Enhanced elicitation of potent neutralizing antibodies by the SARS-CoV-2 spike receptor binding domain Fc fusion protein in mice. Vaccine *38*, 7205–7212.

62. Zang, J., Gu, C., Zhou, B., Zhang, C., Yang, Y., Xu, S., Zhang, X., Zhou, Y., Bai, L., Wu, Y., et al. (2020). Immunization with the receptor–binding domain of SARS-CoV-2 elicits antibodies cross-neutralizing SARS-CoV-2 and SARS-CoV without antibody-dependent enhancement. Cell Discov. *6*, 61.

63. Tan, H.X., Juno, J.A., Lee, W.S., Barber-Axthelm, I., Kelly, H.G., Wragg, K.M., Esterbauer, R., Amarasena, T., Mordant, F.L., Subbarao, K., et al. (2021). Immunogenicity of prime-boost protein subunit vaccine strategies against SARS-CoV-2 in mice and macaques. Nat. Commun. *12*, 1403.

64. Liang, J.G., Su, D., Song, T.Z., Zeng, Y., Huang, W., Wu, J., Xu, R., Luo, P., Yang, X., Zhang, X., et al. (2021). S-Trimer, a COVID-19 subunit vaccine candidate, induces protective immunity in nonhuman primates. Nat. Commun. *12*, 1346.

65. Mandolesi, M., Sheward, D.J., Hanke, L., Ma, J., Pushparaj, P., Perez Vidakovics, L., Kim, C., Adori, M., Lenart, K., Lore, K., et al. (2021). SARS-CoV-2 protein subunit vaccination of mice and rhesus macaques elicits potent and durable neutralizing antibody responses. Cell Rep. Med. *2*, 100252.

66. Zhang, B., Chao, C.W., Tsybovsky, Y., Abiona, O.M., Hutchinson, G.B., Moliva, J.I., Olia, A.S., Pegu, A., Phung, E., Stewart-Jones, G.B.E., et al. (2020). A platform incorporating trimeric antigens into self-assembling nanoparticles reveals SARS-CoV-2-spike nanoparticles to elicit substantially higher neutralizing responses than spike alone. Sci. Rep. *10*, 18149.

67. Walls, A.C., Fiala, B., Schafer, A., Wrenn, S., Pham, M.N., Murphy, M., Tse, L.V., Shehata, L., O'Connor, M.A., Chen, C., et al. (2020). Elicitation of potent neutralizing antibody responses by designed protein nanoparticle vaccines for SARS-CoV-2. Cell *183*, 1367–1382.

68. Arunachalam, P.S., Walls, A.C., Golden, N., Atyeo, C., Fischinger, S., Li, C., Aye, P., Navarro, M.J., Lai, L., Edara, V.V., et al. (2021). Adjuvanting a subunit COVID-19 vaccine to induce protective immunity. Nature *594*, 253–258.

69. Guebre-Xabier, M., Patel, N., Tian, J.H., Zhou, B., Maciejewski, S., Lam, K., Portnoff, A.D., Massare, M.J., Frieman, M.B., Piedra, P.A., et al. (2020). NVX-CoV2373 vaccine protects cynomolgus macaque upper and lower airways against SARS-CoV-2 challenge. Vaccine *38*, 7892–7896.

70. Brouwer, P.J.M., Brinkkemper, M., Maisonnasse, P., Dereuddre-Bosquet, N., Grobben, M., Claireaux, M., de Gast, M., Marlin, R., Chesnais, V., Diry, S., et al. (2021). Two-component spike nanoparticle vaccine protects macaques from SARS-CoV-2 infection. Cell *184*, 1188–1200.

71. Alving, C.R., Beck, Z., Matyas, G.R., and Rao, M. (2016). Liposomal adjuvants for human vaccines. Expert Opin. Drug Deliv. *13*, 807–816.

72. Nisini, R., Poerio, N., Mariotti, S., De Santis, F., and Fraziano, M. (2018). The multirole of liposomes in therapy and prevention of infectious diseases. Front. Immunol. *9*, 155.

73. Ingale, J., Stano, A., Guenaga, J., Sharma, S.K., Nemazee, D., Zwick, M.B., and Wyatt, R.T. (2016). High-density array of well-ordered HIV-1 spikes on synthetic liposomal nanoparticles efficiently activate B cells. Cell Rep. *15*, 1986–1999.

74. Bale, S., Goebrecht, G., Stano, A., Wilson, R., Ota, T., Tran, K., Ingale, J., Zwick, M.B., and Wyatt, R.T. (2017). Covalent linkage of HIV-1 trimers to synthetic liposomes elicits improved B cell and antibody responses. J. Virol. *91*, e00443–17.

75. Martinez-Murillo, P., Tran, K., Guenaga, J., Lindgren, G., Adori, M., Feng, Y., Phad, G.E., Vazquez Bernat, N., Bale, S., Ingale, J., et al. (2017). Particulate array of well-ordered HIV clade C Env trimers elicits neutralizing antibodies that display a unique V2 cap approach. Immunity *46*, 804–817.

76. Dubrovskaya, V., Tran, K., Ozorowski, G., Guenaga, J., Wilson, R., Bale, S., Cottrell, C.A., Turner, H.L., Seabright, G., O'Dell, S., et al. (2019). Vaccination with glycan-modified HIV NFL envelope trimer-liposomes elicits broadly neutralizing antibodies to multiple sites of vulnerability. Immunity *51*, 915–929.

77. Edwards, R.J., Mansouri, K., Stalls, V., Manne, K., Watts, B., Parks, R., Janowska, K., Gobeil, S.M.C., Kopp, M., Li, D., et al. (2021). Cold sensitivity of the SARS-CoV-2 spike ectodomain. Nat. Struct. Mol. Biol. *28*, 128–131.

78. Eldred, B.E., Dean, A.J., McGuire, T.M., and Nash, A.L. (2006). Vaccine components and constituents: responding to consumer concerns. Med. J. Aust. *184*, 170–175.

79. Hsieh, C.L., Goldsmith, J.A., Schaub, J.M., DiVenere, A.M., Kuo, H.C., Javanmardi, K., Le, K.C., Wrapp, D., Lee, A.G., Liu, Y., et al. (2020). Structure-based design of prefusion-stabilized SARS-CoV-2 spikes. Science *369*, 1501–1505.

80. Xiong, X., Qu, K., Ciazynska, K.A., Hosmillo, M., Carter, A.P., Ebrahimi, S., Ke, Z., Scheres, S.H.W., Bergamaschi, L., Grice, G.L., et al. (2020). A thermostable, closed SARS-CoV-2 spike protein trimer. Nat. Struct. Mol. Biol. *27*, 934–941.

81. Toelzer, C., Gupta, K., Yadav, S.K.N., Borucu, U., Davidson, A.D., Kavanagh Williamson, M., Shoemark, D.K., Garzoni, F., Staufer, O., Milligan, R., et al. (2020). Free fatty acid binding pocket in the locked structure of SARS-CoV-2 spike protein. Science *370*, 725–730.

82. Rosa, A., Pye, V.E., Graham, C., Muir, L., Seow, J., Ng, K.W., Cook, N.J., Rees-Spear, C., Parker, E., Dos Santos, M.S., et al. (2021). SARS-CoV-2 can recruit a heme metabolite to evade antibody immunity. Sci. Adv. *7*, eabg7607.

83. Cohen, A.A., Gnanapragasam, P.N.P., Lee, Y.E., Hoffman, P.R., Ou, S., Kakutani, L.M., Keeffe, J.R., Wu, H.J., Howarth, M., West, A.P., et al. (2021). Mosaic nanoparticles elicit cross-reactive immune responses to zoonotic coronaviruses in mice. Science *371*, 735–741.

84. Tan, T.K., Rijal, P., Rahikainen, R., Keeble, A.H., Schimanski, L., Hussain, S., Harvey, R., Hayes, J.W.P., Edwards, J.C., McLean, R.K., et al. (2021). A COVID-19 vaccine candidate using SpyCatcher multimerization of the SARS-CoV-2 spike protein receptor-binding domain induces potent neutralising antibody responses. Nat. Commun. *12*, 542.

85. Yu, J., Tostanoski, L.H., Peter, L., Mercado, N.B., McMahan, K., Mahrokhian, S.H., Nkolola, J.P., Liu, J., Li, Z., Chandrashekar, A., et al. (2020). DNA vaccine protection against SARS-CoV-2 in rhesus macaques. Science *369*, 806–811.

86. Addetia, A., Crawford, K.H.D., Dingens, A., Zhu, H., Roychoudhury, P., Huang, M.L., Jerome, K.R., Bloom, J.D., and Greninger, A.L. (2020).

Neutralizing antibodies correlate with protection from SARS-CoV-2 in humans during a fishery vessel outbreak with a high attack rate. J. Clin. Microbiol. *58*, e02107–e02120.

87. Keech, C., Albert, G., Cho, I., Robertson, A., Reed, P., Neal, S., Plested, J.S., Zhu, M., Cloney-Clark, S., Zhou, H., et al. (2020). Phase 1-2 trial of a SARS-CoV-2 recombinant spike protein nanoparticle vaccine. N. Engl. J. Med. *383*, 2320–2332.
88. Sahin, U., Muik, A., Derhovanessian, E., Vogler, I., Kranz, L.M., Vormehr, M., Baum, A., Pascal, K., Quandt, J., Maurus, D., et al. (2020). COVID-19 vaccine BNT162b1 elicits human antibody and TH1 T cell responses. Nature *586*, 594–599.
89. Ewer, K.J., Barrett, J.R., Belij-Rammerstorfer, S., Sharpe, H., Makinson, R., Morter, R., Flaxman, A., Wright, D., Bellamy, D., Bittaye, M., et al. (2021). T cell and antibody responses induced by a single dose of ChAdOx1 nCoV-19 (AZD1222) vaccine in a phase 1/2 clinical trial. Nat. Med. *27*, 270–278.
90. Ganneru, B., Jogdand, H., Daram, V.K., Das, D., Molugu, N.R., Prasad, S.D., Kannappa, S.V., Ella, K.M., Ravikrishnan, R., Awasthi, A., et al. (2021). Th1 skewed immune response of whole virion inactivated SARS CoV 2 vaccine and its safety evaluation. iScience *24*, 102298.
91. Pisanic, N., Randad, P.R., Kruczynski, K., Manabe, Y.C., Thomas, D., Pekosz, A., Klein, S., Betenbaugh, M.J., Clarke, W.A., Laeyendecker, O., et al. (2020). COVID-19 serology at population scale: SARS-CoV-2-specific antibody responses in saliva. J. Clin. Microbiol. *59*, e02204–e02220.
92. Suthar, M.S., Zimmerman, M.G., Kauffman, R.C., Mantus, G., Linderman, S.L., Hudson, W.H., Vanderheiden, A., Nyhoff, L., Davis, C.W., Adekunle, O., et al. (2020). Rapid generation of neutralizing antibody responses in COVID-19 patients. Cell Rep. Med. *1*, 100040.
93. Stamatatos, L., Czartoski, J., Wan, Y.H., Homad, L.J., Rubin, V., Glantz, H., Neradilek, M., Seydoux, E., Jennewein, M.F., MacCamy, A.J., et al. (2021). mRNA vaccination boosts cross-variant neutralizing antibodies elicited by SARS-CoV-2 infection. Science *372*, 1413–1418.
94. Barnes, C.O., Jette, C.A., Abernathy, M.E., Dam, K.A., Esswein, S.R., Gristick, H.B., Malyutin, A.G., Sharaf, N.G., Huey-Tubman, K.E., Lee, Y.E., et al. (2020). SARS-CoV-2 neutralizing antibody structures inform therapeutic strategies. Nature *588*, 682–687.
95. Barnes, C.O., West, A.P., Jr., Huey-Tubman, K.E., Hoffmann, M.A.G., Sharaf, N.G., Hoffman, P.R., Koranda, N., Gristick, H.B., Gaebler, C., Muecksch, F., et al. (2020). Structures of human antibodies bound to SARS-CoV-2 spike reveal common epitopes and recurrent features of antibodies. Cell *182*, 828–842.
96. Kreye, J., Reincke, S.M., Kornau, H.C., Sanchez-Sendin, E., Corman, V.M., Liu, H., Yuan, M., Wu, N.C., Zhu, X., Lee, C.D., et al. (2020). A therapeutic non-self-reactive SARS-CoV-2 antibody protects from lung pathology in a COVID-19 Hamster model. Cell *183*, 1058–1069.
97. Korber, B., Fischer, W.M., Gnanakaran, S., Yoon, H., Theiler, J., Abfalterer, W., Hengartner, N., Giorgi, E.E., Bhattacharya, T., Foley, B., et al. (2020). Tracking changes in SARS-CoV-2 spike: evidence that D614G increases infectivity of the COVID-19 virus. Cell *182*, 812–827.
98. Zhang, J., Cai, Y., Xiao, T., Lu, J., Peng, H., Sterling, S.M., Walsh, R.M., Jr., Rits-Volloch, S., Zhu, H., Woosley, A.N., et al. (2021). Structural impact on SARS-CoV-2 spike protein by D614G substitution. Science *372*, 525–530.
99. Ozono, S., Zhang, Y., Ode, H., Sano, K., Tan, T.S., Imai, K., Miyoshi, K., Kishigami, S., Ueno, T., Iwatani, Y., et al. (2021). SARS-CoV-2 D614G spike mutation increases entry efficiency with enhanced ACE2-binding affinity. Nat. Commun. *12*, 848.
100. Zhang, L., Jackson, C.B., Mou, H., Ojha, A., Peng, H., Quinlan, B.D., Rangarajan, E.S., Pan, A., Vanderheiden, A., Suthar, M.S., et al. (2020). SARS-CoV-2 spike-protein D614G mutation increases virion spike density and infectivity. Nat. Commun. *11*, 6013.
101. Gobeil, S.M., Janowska, K., McDowell, S., Mansouri, K., Parks, R., Stalls, V., Kopp, M.F., Manne, K., Li, D., Wiehe, K., et al. (2021). Effect of natural mutations of SARS-CoV-2 on spike structure, conformation, and antigenicity. Science *373*, eabi6226.
102. Cai, Y., Zhang, J., Xiao, T., Lavine, C.L., Rawson, S., Peng, H., Zhu, H., Anand, K., Tong, P., Gautam, A., et al. (2021). Structural basis for enhanced infectivity and immune evasion of SARS-CoV-2 variants. Science *373*, 642–648.
103. Yuan, M., Huang, D., Lee, C.D., Wu, N.C., Jackson, A.M., Zhu, X., Liu, H., Peng, L., van Gils, M.J., Sanders, R.W., et al. (2021). Structural and functional ramifications of antigenic drift in recent SARS-CoV-2 variants. Science *373*, 818–823.
104. Weissman, D., Alameh, M.G., de Silva, T., Collini, P., Hornsby, H., Brown, R., LaBranche, C.C., Edwards, R.J., Sutherland, L., Santra, S., et al. (2021). D614G spike mutation increases SARS CoV-2 susceptibility to neutralization. Cell Host Microbe *29*, 23–31.
105. Zhou, D., Dejnirattisai, W., Supasa, P., Liu, C., Mentzer, A.J., Ginn, H.M., Zhao, Y., Duyvesteyn, H.M.E., Tuekprakhon, A., Nutalai, R., et al. (2021). Evidence of escape of SARS-CoV-2 variant B.1.351 from natural and vaccine-induced sera. Cell *184*, 2348–2361.
106. Dejnirattisai, W., Zhou, D., Supasa, P., Liu, C., Mentzer, A.J., Ginn, H.M., Zhao, Y., Duyvesteyn, H.M.E., Tuekprakhon, A., Nutalai, R., et al. (2021). Antibody evasion by the P.1 strain of SARS-CoV-2. Cell *184*, 2939–2954.
107. Hoffmann, M., Arora, P., Gross, R., Seidel, A., Hornich, B.F., Hahn, A.S., Kruger, N., Graichen, L., Hofmann-Winkler, H., Kempf, A., et al. (2021). SARS-CoV-2 variants B.1.351 and P.1 escape from neutralizing antibodies. Cell *184*, 2384–2393.
108. Edara, V.V., Norwood, C., Floyd, K., Lai, L., Davis-Gardner, M.E., Hudson, W.H., Mantus, G., Nyhoff, L.E., Adelman, M.W., Fineman, R., et al. (2021). Infection- and vaccine-induced antibody binding and neutralization of the B.1.351 SARS-CoV-2 variant. Cell Host Microbe *29*, 516–521.
109. Garcia-Beltran, W.F., Lam, E.C., St Denis, K., Nitido, A.D., Garcia, Z.H., Hauser, B.M., Feldman, J., Pavlovic, M.N., Gregory, D.J., Poznansky, M.C., et al. (2021). Multiple SARS-CoV-2 variants escape neutralization by vaccine-induced humoral immunity. Cell *184*, 2372–2383.
110. Kuzmina, A., Khalaila, Y., Voloshin, O., Keren-Naus, A., Boehm-Cohen, L., Raviv, Y., Shemer-Avni, Y., Rosenberg, E., and Taube, R. (2021). SARS-CoV-2 spike variants exhibit differential infectivity and neutralization resistance to convalescent or post-vaccination sera. Cell Host Microbe *29*, 522–528.
111. Geers, D., Shamier, M.C., Bogers, S., den Hartog, G., Gommers, L., Nieuwkoop, N.N., Schmitz, K.S., Rijsbergen, L.C., van Osch, J.A.T., Dijkhuizen, E., et al. (2021). SARS-CoV-2 variants of concern partially escape humoral but not T-cell responses in COVID-19 convalescent donors and vaccinees. Sci. Immunol. *6*, eabj1750.
112. Rees-Spear, C., Muir, L., Griffith, S.A., Heaney, J., Aldon, Y., Snitselaar, J.L., Thomas, P., Graham, C., Seow, J., Lee, N., et al. (2021). The effect of spike mutations on SARS-CoV-2 neutralization. Cell Rep. *34*, 108890.
113. Supasa, P., Zhou, D., Dejnirattisai, W., Liu, C., Mentzer, A.J., Ginn, H.M., Zhao, Y., Duyvesteyn, H.M.E., Nutalai, R., Tuekprakhon, A., et al. (2021). Reduced neutralization of SARS-CoV-2 B.1.1.7 variant by convalescent and vaccine sera. Cell *184*, 2201–2211.e7.
114. Greaney, A.J., Loes, A.N., Crawford, K.H.D., Starr, T.N., Malone, K.D., Chu, H.Y., and Bloom, J.D. (2021). Comprehensive mapping of mutations in the SARS-CoV-2 receptor-binding domain that affect recognition by polyclonal human plasma antibodies. Cell Host Microbe *29*, 463–476.
115. Caniels, T.G., Bontjer, I., van der Straten, K., Poniman, M., Burger, J.A., Appelman, B., Lavell, H.A.A., Oomen, M., Godeke, G.J., Valle, C., et al. (2021). Emerging SARS-CoV-2 variants of concern evade humoral immune responses from infection and vaccination. Sci. Adv. *7*, eabj5365.
116. Sokal, A., Chappert, P., Barba-Spaeth, G., Roeser, A., Fourati, S., Azzaoui, I., Vandenberghe, A., Fernandez, I., Meola, A., Bouvier-Alias, M., et al. (2021). Maturation and persistence of the anti-SARS-CoV-2 memory B cell response. Cell *184*, 1201–1213.

117. Gaebler, C., Wang, Z., Lorenzi, J.C.C., Muecksch, F., Finkin, S., Tokuyama, M., Cho, A., Jankovic, M., Schaefer-Babajew, D., Oliveira, T.Y., et al. (2021). Evolution of antibody immunity to SARS-CoV-2. Nature *591*, 639–644.

118. Goel, R.R., Painter, M.M., Apostolidis, S.A., Mathew, D., Meng, W., Rosenfeld, A.M., Lundgreen, K.A., Reynaldi, A., Khoury, D.S., Pattekar, A., et al. (2021). mRNA vaccination induces durable immune memory to SARS-CoV-2 with continued evolution to variants of concern. Science *374*, eabm0829.

119. Schmidt, F., Weisblum, Y., Muecksch, F., Hoffmann, H.H., Michailidis, E., Lorenzi, J.C.C., Mendoza, P., Rutkowska, M., Bednarski, E., Gaebler, C., et al. (2020). Measuring SARS-CoV-2 neutralizing antibody activity using pseudotyped and chimeric viruses. J. Exp. Med. *217*, e20201181.

120. Lescure, F.X., Bouadma, L., Nguyen, D., Parisey, M., Wicky, P.H., Behillil, S., Gaymard, A., Bouscambert-Duchamp, M., Donati, F., Le Hingrat, Q., et al. (2020). Clinical and virological data of the first cases of COVID-19 in Europe: a case series. Lancet Infect. Dis. *20*, 697–706.

121. Lai, R.P.J., Hock, M., Radzimanowski, J., Tonks, P., Lutje Hulsik, D., Effantin, G., et al. (2014). A fusion intermediate gp41 immunogen elicits neutralizing antibodies to HIV-1. J. Biol. Chem. *289*, 29912–29926.

122. Scheres, S.H. (2012). RELION: implementation of a Bayesian approach to cryo-EM structure determination. J. Struct. Biol. *180*, 519–530.

123. Mastronarde, D.N. (2005). Automated electron microscope tomography using robust prediction of specimen movements. J. Struct. Biol. *152*, 36–51.

124. Zheng, S.Q., Palovcak, E., Armache, J.P., Verba, K.A., Cheng, Y., and Agard, D.A. (2017). MotionCor2: anisotropic correction of beam-induced motion for improved cryo-electron microscopy. Nat. Methods *14*, 331–332.

125. Zivanov, J., Nakane, T., Forsberg, B.O., Kimanius, D., Hagen, W.J., Lindahl, E., and Scheres, S.H. (2018). New tools for automated high-resolution cryo-EM structure determination in RELION-3. Elife *7*, e42166.

126. Zhang, K. (2016). Gctf: real-time CTF determination and correction. J. Struct. Biol. *193*, 1–12.

127. Cardone, G., Heymann, J.B., and Steven, A.C. (2013). One number does not fit all: mapping local variations in resolution in cryo-EM reconstructions. J. Struct. Biol. *184*, 226–236.

128. Sanchez-Garcia, R., Gomez-Blanco, J., Cuervo, A., Carazo, J.M., Sorzano, C.O.S., and Vargas, J. (2021). DeepEMhancer: a deep learning solution for cryo-EM volume post-processing. Commun. Biol. *4*, 874.

129. Pettersen, E.F., Goddard, T.D., Huang, C.C., Couch, G.S., Greenblatt, D.M., Meng, E.C., and Ferrin, T.E. (2004). UCSF Chimera–a visualization system for exploratory research and analysis. J. Comput. Chem. *25*, 1605–1612.

130. Adams, P.D., Afonine, P.V., Bunkoczi, G., Chen, V.B., Davis, I.W., Echols, N., Headd, J.J., Hung, L.W., Kapral, G.J., Grosse-Kunstleve, R.W., et al. (2010). PHENIX: a comprehensive Python-based system for macromolecular structure solution. Acta Crystallogr. D Biol. Crystallogr. *66*, 213–221.

131. Emsley, P., Lohkamp, B., Scott, W.G., and Cowtan, K. (2010). Features and development of coot. Acta Crystallogr. D Biol. Crystallogr. *66*, 486–501.

132. Williams, C.J., Headd, J.J., Moriarty, N.W., Prisant, M.G., Videau, L.L., Deis, L.N., Verma, V., Keedy, D.A., Hintze, B.J., Chen, V.B., et al. (2018). MolProbity: more and better reference data for improved all-atom structure validation. Protein Sci. *27*, 293–315.

133. Goddard, T.D., Huang, C.C., Meng, E.C., Pettersen, E.F., Couch, G.S., Morris, J.H., and Ferrin, T.E. (2018). UCSF ChimeraX: meeting modern challenges in visualization and analysis. Protein Sci. *27*, 14–25.

134. Corman, V.M., Landt, O., Kaiser, M., Molenkamp, R., Meijer, A., Chu, D.K., Bleicker, T., Brunink, S., Schneider, J., Schmidt, M.L., et al. (2020). Detection of 2019 novel coronavirus (2019-nCoV) by real-time RT-PCR. Euro Surveill. *25*, 2000045.

135. Wolfel, R., Corman, V.M., Guggemos, W., Seilmaier, M., Zange, S., Muller, M.A., Niemeyer, D., Jones, T.C., Vollmar, P., Rothe, C., et al. (2020). Virological assessment of hospitalized patients with COVID-2019. Nature *581*, 465–469.

136. Shi, R., Shan, C., Duan, X., Chen, Z., Liu, P., Song, J., Song, T., Bi, X., Han, C., Wu, L., et al. (2020). A human neutralizing antibody targets the receptor-binding site of SARS-CoV-2. Nature *584*, 120–124.

137. Pan, F., Ye, T., Sun, P., Gui, S., Liang, B., Li, L., Zheng, D., Wang, J., Hesketh, R.L., Yang, L., et al. (2020). Time course of lung changes at chest CT during recovery from coronavirus disease 2019 (COVID-19). Radiology *295*, 715–721.

STAR★METHODS

KEY RESOURCES TABLE

REAGENT or RESOURCE	SOURCE	IDENTIFIER
Antibodies		
Horsedish peroxidase conjugated goat anti-monkey H+L	Invitrogen	Cat# PA1-84631
Anti-IL2 PerCP5.5 (MQ1-17H12)	BD Bioscience	Cat# 560708
Anti-IL17a Alexa700 (N49-653)	BD Bioscience	Cat# 560613
Anti-IFN-γ V450 (B27)	BD Bioscience	Cat# 560371
Anti-TNF-α BV605 (Mab11)	Biolegend	Cat# 502936
Anti-IL-13 BV711 (JES10-5A2)	BD Bioscience	Cat# 564288
Anti-CD137 APC (4B4)	BD Bioscience	Cat# 550890; RRID:AB_2848292
Anti-CD154 FITC (TRAP1)	BD Bioscience	Cat# 555699; RRID:AB_396049
CD3 APC-Cy7 (SP34-2)	BD Bioscience	Cat# 557757; RRID:AB_396863
CD4 BV510 (L200)	BD Bioscience	Cat# 563094
CD8 PE-Vio770 (BW135/80)	Miltenyi Biotec	Cat# 130-113-721
FastImmune ™ CD28/CD49d	BD Bioscience	Cat# 130-113-159
Live/Dead Fixable Blue Dead Cell	Thermofisher	Cat# L34962
Anti-Monkey IgG (γ-chain specific)-Biotin antibody produced in goat	Sigma Aldrich	Cat# SAB3700768
Anti-Monkey IgA (α-chain specific)-Biotin antibody produced in goat	Sigma Aldrich	Cat# SAB3700761
Bacterial and virus strains		
SARS-CoV-2 (hCoV-19/France/IDF0372/2020 strain)	Lescure et al.[119]	EPI_ISL_410720 (GISAID ID)
TOP10 Chemically Competent *E. coli*	Thermofisher	C404010
Chemicals, peptides, and recombinant proteins		
Formaldehyde solution 36.5%	Sigma-Aldrich	Cat# F8775-25ML
Dithiothreitol	Sigma-Aldrich	Cat# 43819
Streptavidin-PE	ThermoFisher Scientific	Cat# 12-4317-87
EDC	ThermoFisher Scientific	Cat# A35391
Sulfo-NHS	ThermoFisher Scientific	Cat# A39269
Ampiciline	Euromedex	Cat# EU0400-D
Polyethylemine (PEI-25K)	Polyscience	Cat# 23966-1
L-α-phosphatidylcholine (PC)	Avanti Polar Lipids	840051
DGS-NTA(Ni)	Avanti Polar Lipids	790404
Cholesterol	Avanti Polar Lipids	700000
Bradford Protein Assay Reactive	BioRad	Cat# 5000006
Excel purification resin	Cytiva	Cat# 17-3712-01
PBS 10X	EuroMedex	Cat# ET330-A
Penicillin	Sigma-Aldrich	Cat# P3032-10MI
Streptomycin	VWR	Cat# 382-EU-100G
MPLA liposomes	Polymun Scientific	https://www.polymun.com/liposomes/reference-projects/
Bovine Serum Albumin	Sigma-Aldrich	Cat# A2153-1000
GlutaMax	Gibco	Cat# 35050061
PepMix™ SARS-CoV-2 (Spike Glycoprotein)	JPT peptide Technologies	Cat# PM-WCPV-S
Poly-L-Lysine Hydrobromide	Sigma-Aldrich	Cat# P1399

(*Continued on next page*)

Continued

REAGENT or RESOURCE	SOURCE	IDENTIFIER
Critical commercial assays		
SSIV Reverse Transcriptase	Thermo Fisher scientific	Cat# 18090050
Ligation Sequencing Kit	Nanopore	Cat# SQK-LSK109
Q5 Hot Start DNA Polymerase	NEB	Cat# M0494
Expi293™ Expression System Kit	Thermo Fisher scientific	Cat# A14635
Nano-Glo Luciferase Assay System	Promega	Cat# N1130
Nucleospin 96 Virus Core	Macharey-Nagel	Cat# 740452.4
Experimental models: Cell lines		
FreeStyle™ 293-F Cells	Thermo Fisher scientific	Cat# R79007
Expi293F™ Cells	Thermo Fisher scientific	Cat# A14527
VeroE6	ATCC	ATTC®CRL 1586TM
HEK293T/ACE2 cells	Schmidt et al.[120]	N/A
Desposited data		
PDB	7Q1Z	https://www.rcsb.org/
EMBD	EMD-13776	https://www.ebi.ac.uk/emdb/
Experimental models: Organisms/strains		
Cynomolgus macaques	Cynologics	N/A
Oligonucleotides		
Primers covid19 V3	ARTIC network	http://artic.network/resources/ncov-amplicon-v3.pdf
RdRp-IP4 primer, forward – GGTAACTGGTATGATTTCG	https://www.who.int/docs/default-source/coronaviruse/real-time-rt-pcr-assays-for-the-detection-of-sars-cov-2-institut-pasteur-paris.pdf?sfvrsn=3662fcb6_2	N/A
RdRp-IP4 primer, reverse - CTGGTCAAGGTTAATATAGG	https://www.who.int/docs/default-source/coronaviruse/real-time-rt-pcr-assays-for-the-detection-of-sars-cov-2-institut-pasteur-paris.pdf?sfvrsn=3662fcb6_2	N/A
RdRp-IP4 primer probe P - TCATACAAACCACGCCAG G	https://www.who.int/docs/default-source/coronaviruse/real-time-rt-pcr-assays-for-the-detection-of-sars-cov-2-institut-pasteur-paris.pdf?sfvrsn=3662fcb6_2	N/A
sgLead SARSCoV2-forward - CGATCTCTTGTAGATCTGTTCTC	Corman[121]	N/A
E-Sarbeco-reverse primer - ATATTGCAGCAGTACGCACACA	Corman[121]	N/A
E-Sarbeco probe HEX-ACACTAGCCATCCTTACTGCGCTTCG-BHQ1	Corman[121]	N/A
Recombinant DNA		
Plasmid: Protein S	Wrapp et al.[8]	N/A
Plasmid: RBD	NR-52309, BEI resources, NIAID, NIH	N/A
pHIV-1NL43ΔENV-NanoLuc plasmid	Schmidt et al.[120]	N/A
SARS-CoV-2-SΔ19 plasmid	Schmidt et al.[120]	N/A
gBlock B.1.1.7, B.1.351, and P.1	Integrated DNA Technologies	N /A
Variants : B.1.1.7, B.1.351, and P.1 cloned in pCR3 plasmid	Caniels et al.[115]	N/A

(*Continued on next page*)

Continued

REAGENT or RESOURCE	SOURCE	IDENTIFIER
Software and algorithms		
GraphPad Prism v7	GraphPad	N/A
GraphPad Prism v8	GraphPad	N/A
ProtParam		http://web.expasy.org/
Prometheus MT	Nanotemper	https://nanotempertech.com/prometheus/
Flowjo v10	Flowjo	N/A
INTELLISPACE PORTAL 8 software	Philips Healthcare	https://www.philips.fr/healthcare/product/HC881062/intellispace-portal-80-all-your-advanced-analysis-needs-one-comprehensive-solution
SerialEM	Mastronarde et al.[122]	N/A
motioncor2	Zheng et al.[123]	N/A
RELION 3.1.2	Zivanov et al.[124]	N/A
GCTF	Zhang et al.[125]	N/A
Blocres	Cardone et al.[126]	N/A
DeepEMhancer	Sanchez-Garcia et al.[127]	N/A
CHIMERA	Pettersen et al.[128]	N/A
COOT	Emsley et al.[129]	N/A
MOLPROBITY	Williams et al.[130]	N/A
PHENIX	Adams et al.[131]	N/A
CHIMERAX	Goddard et al.[132]	N/A
Others		
Superose 6 increase	GE Healthcare	28-9909-44
Superdex 75	GE Healthcare	N/A
Whatman® Nuclepore™ Track-Etched Membranes	Merck	**WHA111105**
FreeStyle Expression Medium	Thermo Scientific	Cat# 12338018
Opti-MEM™ I Reduced Serum Medium	Thermo Scientific	Cat#31985062
RPMI Medium 1640	GIBCO	Cat# 21875-034
DMEM	Sigma-Aldrich	Cat# D6429-500ML
Grilles Cu 400 mesh	Oxford Instruments	G2400C
NucleoBond PC 2000 EF	Macherey Nagel	Cat# 740549
NucleoBond Xtra Midi EF	Macherey Nagel	Cat# 740420
Nucleobond Xtra Mini Kit	Macherey-Nagel	N/A
ELISA microplates	Thermo Scientific	10547781
Protein A Sepharose ®	Abcam	Cat# ab193256
Protein G Sepharose ™	Abcam	Cat# ab17061801
Instant Blue Coomassie Protein Stain	Abcam	Cat# ab119211
Amicon® Ultra-15	Sigma-Aldrich	UFC903096
Amicon® Ultra-30	Sigma-Aldrich	UFC901096
Capillars		N/A
AKTA system	GE Healthcare	https://www.cytivalifesciences.com/en/us/shop/chromatography/chromatography-systems/akta-pure-p-05844
TMB	Interchim	UP 664781
Glomax	Turner BioSystems	Model# 9101-002
Microplate 96 well half area white	Greiner bio-one	Cat# 675074

(*Continued on next page*)

Continued

REAGENT or RESOURCE	SOURCE	IDENTIFIER
Greiner CELLSTAR® 96 well plates, round bottom clear wells	Merck	Cat# M9436
Greiner CELLSTAR® 96 well plates, flat bottom clear wells	Merck	Cat# M0812
MagPlex-C Microspheres 1 mL	Luminex	Cat# MC100XX-01
MAGPIX	Luminex	Cat# MAGPIX-XPON4.1-RUO

RESOURCE AVAILABILITY

Lead contact

Further information and requests for resources and reagents should be directed to and will be fulfilled by the Lead Contact, Winfried Weissenhorn (winfried.weissenhorn@ibs.fr).

Materials availability

All reagents will be made available from the Lead Contact on request and after completion of a Materials Transfer Agreement.

Data and code availability

Data: The raw data supporting the findings of the study are available from the lead contact upon request. Structural data have been deposited at https://www.rcsb.org/ and https://www.ebi.ac.uk/emdb/. They are publicly available as of the date of publication. Accession codes are listed in the key resources table.

Code: This paper does not report original code

General statement: Any additional information required to reanalyze the data reported in this paper is available from the Lead Contact upon request.

EXPERIMENTAL MODEL AND SUBJECT DETAILS

Cell lines

HEK293T (ATCC CRL-11268)[115] and HEK293F (Thermo Fisher Scientific) and are human embryonic kidney cell lines. HEK293F cells are adapted to grow in suspension. HEK293F cells were cultured at 37°C with 8% CO_2 and shaking at 125 rpm in 293FreeStyle expression medium (Life Technologies). HEK293T cells were cultured at 37°C with 5% CO_2 in flasks with DMEM supplemented with 10% fetal bovine serum (FBS), streptomycin (100 μg/mL) and penicillin (100 U/mL). HEK293T/ACE2 cells[119] are a human embryonic kidney cell line expressing human angiotensin-converting enzyme 2. HEK293T/ACE2 cells were cultured at 37°C with 5% CO_2 in flasks with DMEM supplemented with 10% FBS, streptomycin (100 μg/mL) and penicillin (100 U/mL). VeroE6 cells (ATCC CRL-1586) are a kidney epithelial cells from African green monkeys. VeroE6 cells were cultured at 37°C with 5% CO_2 in DMEM supplemented with or without streptomycin (100 μg/mL) and penicillin (100 U/mL) and with or without 5 or 10% FBS, and with or without TPCK-trypsin. PBMC were isolated from macaque sera and cultured in RPMI1640 Glutamax+ medium (Gibco) supplemented with 10 % FBS.

Viruses

SARS-CoV-2 virus (hCoV-19/France/ IDF0372/2020 strain) was isolated by the National Reference Center for Respiratory Viruses (Institut Pasteur, Paris, France) as previously described[120] and produced by two passages on Vero E6 cells in DMEM (Dulbecco's Modified Eagles Medium) without FBS, supplemented with 1% P/S (penicillin at 10,000 U ml^{-1} and streptomycin at 10,000 μg ml^{-1}) and 1 μg ml^{-1} TPCK-trypsin at 37 °C in a humidified CO_2 incubator and titrated on Vero E6 cells. Whole genome sequencing was performed as described[120] with no modifications observed compared with the initial specimen and sequences were deposited after assembly on the GISAID EpiCoV platform under accession number ID EPI_ISL_410720.

Ethics and biosafety statement

Cynomolgus macaques (*Macaca fascicularis*) originating from Mauritian AAALAC certified breeding centers were used in this study. MF1-MF4, vaccinated group and MF5-MF8, control group.

	Gender	Date of birth	Age (years)	Weight at Day 0 post exposure (kg)	Developmental stage
MF1	M	04/04/2017	3,68	3,96	Young adult
MF2	M	05/04/2017	3,68	4,52	Young adult
MF3	M	10/04/2017	3,67	4,98	Young adult

(*Continued on next page*)

Continued

	Gender	Date of birth	Age (years)	Weight at Day 0 post exposure (kg)	Developmental stage
MF4	M	12/04/2017	3,66	6,39	Young adult
MF5	M	27/04/2017	3,62	3,64	Young adult
MF6	M	27/04/2017	3,62	4,29	Young adult
MF7	M	12/05/2017	3,58	3,14	Young adult
MF8	M	15/05/2017	3,57	3,91	Young adult

All animals were housed in IDMIT infrastructure facilities (CEA, Fontenay-aux-roses), under BSL-2 and BSL-3 containment when necessary (Animal facility authorization #D92-032-02, Préfecture des Hauts de Seine, France) and in compliance with European Directive 2010/63/EU, the French regulations and the Standards for Human Care and Use of Laboratory Animals, of the Office for Laboratory Animal Welfare (OLAW, assurance number #A5826-01, US). The protocols were approved by the institutional ethical committee ''Comité d'Ethique en Expérimentation Animale du Commissariat à l'Energie Atomique et aux Energies Alternatives'' (CE-tEA #44) under statement number A20-011. The study was authorized by the ''Research, Innovation and Education Ministry'' under registration number APAFIS#24434-2020030216532863.

Animals and study design

Cynomolgus macaques were randomly assigned in two experimental groups. The vaccinated group (n = 4) received 50 μg of SARS CoV-2 S-LV adjuvanted with 500 μg of MPLA liposomes (Polymun Scientific, Klosterneuburg, Austria) diluted in PBS at weeks 0, 4, 8 and 19, while control animals (n = 4) received no vaccination. Vaccinated animals were sampled in blood at weeks 0, 2, 4, 6, 8, 10, 12, 14, 19, 21 and 22. At week 24, all animals were exposed to a total dose of 10^5 pfu of SARS-CoV-2 virus (hCoV-19/France/ IDF0372/ 2020 strain; GISAID EpiCoV platform under accession number EPI_ISL_410720) via the combination of intranasal and intra-tracheal routes (0,25 mL in each nostril and 4,5 mL in the trachea, i.e., a total of 5 mL; day 0), using atropine (0.04 mg/kg) for pre-medication and ketamine (5 mg/kg) with medetomidine (0.042 mg/kg) for anesthesia. Nasopharyngeal, tracheal and rectal swabs, were collected at days 2, 3, 4, 6, 7, 10, 14 and 27 days past exposure (dpe) while blood was taken at days 2, 4, 7, 10, 14 and 27 dpe. Bronchoalveolar lavages (BAL) were performed using 50 mL sterile saline on 3 and 7 dpe. Chest CT was performed at 3, 7, 10 and 14 dpe in anesthetized animals using tiletamine (4 mg kg^{-1}) and zolazepam (4 mg kg^{-1}). Blood cell counts, haemoglobin, and haematocrit, were determined from EDTA blood using a DHX800 analyzer (Beckman Coulter).

METHODS DETAILS

Protein expression and purification

The SARS-CoV-2 S gene encoding residues 1-1208 with proline substitutions at residues 986 and 987 (''2P''), a ''GSAS'' substitution at the furin cleavage site (residues 682-685) a C-terminal T4 fibritin trimerization motif, an HRV3C protease cleavage site, a TwinStrepTag and Hexa-His-tag[8] was transiently expressed in FreeStyle293F cells (Thermo Fisher scientific) using polyethylenimine (PEI) 1 μg/μl for transfection. Supernatants were harvested five days post-transfection, centrifuged for 30 min at 5000 rpm and filtered using 0.20 μm filters (ClearLine®). SARS-CoV-2 S protein was purified from the supernatant by Ni^{2+}-Sepharose chromatography (Excel purification resin, Cytiva) in buffer A (50 mM HEPES pH 7.4, 200 mM NaCl) and eluted in buffer B (50 mM HEPES pH 7.4, 200 mM NaCl, 500 mM imidazole). Eluted SARS-CoV-2 S containing fractions were concentrated using Amicon Ultra (cut-off: 30 KDa) (Millipore) and further purified by size-exclusion chromatography (SEC) on a Superose 6 column (GE Healthcare) in buffer A or in PBS.

For RBD expression, the following reagent was produced under HHSN272201400008C and obtained through BEI Resources, NIAID, NIH: Vector pCAGGS containing the SARS-Related Coronavirus 2, Wuhan-Hu-1 Spike Glycoprotein Receptor Binding Domain (RBD), NR-52309. The SARS-CoV-2 S RBD domain (residues 319 to 541) was expressed in EXPI293 cells by transient transfection according to the manufacturer's protocol (Thermo Fisher Scientific). Supernatants were harvested five days after transfection and cleared by centrifugation. The supernatant was passed through a 0.45 μm filter and RBD was purified using Ni^{2+}-chromatography (HisTrap HP column, GE Healthcare) in buffer C (20 mM Tris pH 7.5 and 150 mM NaCl buffer) followed by a washing step with buffer D (20 mM Tris pH 7.5 and 150 mM NaCl buffer, 75 mM imidazole) and elution with buffer E (20 mM Tris pH 7.5 and 150 mM NaCl buffer, 500 mM imidazole). Eluted RBD was further purified by SEC on a Superdex 75 column (GE Healthcare) in buffer C. Protein concentrations were determined using absorption coefficients at 280 nm calculated with ProtParam (https://web.expasy.org/).

SARS-CoV-2 S crosslinking

S protein at 1 mg/ml in PBS was cross-linked with 4% formaldehyde (FA) (Sigma) overnight at room temperature. The reaction was stopped with 1 M Tris HCl pH 7.4 adjusting the sample buffer to 7.5 mM Tris/HCl pH 7.4. FA was removed by PBS buffer exchange using 30 KDa cut-off concentrators (Amicon). FA crosslinking was confirmed by separating SARS-CoV-2 FA-S on a 10% SDS-PAGE under reducing conditions.

S protein coupling to liposomes

Liposomes for conjugating S protein were prepared as described previously[121] with modifications. Briefly, liposomes were composed of 60% of L-α-phosphatidylcholine, 4% His tag-conjugating lipid, DGS-NTA-(Ni^{2+}) and 36% cholesterol (Avanti Polar Lipids). Lipid components were dissolved in chloroform, mixed and placed for two hours in a desiccator under vacuum at room temperature to obtain a lipid film. The film was hydrated in filtered (0.22 μm) PBS and liposomes were prepared by extrusion using membrane filters with a pore size of 0.1 μm (Whatman Nuclepore Track-Etch membranes). The integrity and size of the liposomes was analyzed by negative staining-EM. For protein coupling, the liposomes were incubated overnight with FA-S or S protein in a 3:1 ratio (w/w). Free FA-S protein was separated from the FA-S-proteoliposomes (S-LVs) by sucrose gradient (5-40%) centrifugation in a SW55 rotor at 40,000 rpm for 2 h. The amount of protein conjugated to the liposomes was determined by Bradford assay and SDS-PAGE densitometry analysis comparing S-LV bands with standard S protein concentrations.

S protein thermostability

Thermal denaturation of SARS-CoV-2 S, native or FA-cross-linked was analyzed by differential scanning fluorimetry coupled to back scattering using a Prometheus NT.48 instrument (Nanotemper Technologies, Munich, DE). Protein samples were first extensively dialyzed against PBS pH 7.4, and the protein concentration was adjusted to 0.3 mg/ml. 10 μL of sample were loaded into the capillary and intrinsic fluorescence was measured at a ramp rate of 1°C/min with an excitation power of 30 %. Protein unfolding was monitored by the changes in fluorescence emission at 350 and 330 nm. The thermal unfolding midpoint (Tm) of the proteins was determined using the Prometheus NT software.

Negative stain electron microscopy

Protein samples were visualized by negative-stain electron microscopy (EM) using 3-4 μL aliquots containing 0.1-0.2 mg/ml of protein. Samples were applied for 10 s onto a mica carbon film and transferred to 400-mesh Cu grids that had been glow discharged at 20 mA for 30 s and then negatively stained with 2% (wt/vol) Uranyl Acetate (UAc) for 30 s. Data were collected on a FEI Tecnai T12 LaB6-EM operating at 120 kV accelerating voltage at 23k magnification (pixel size of 2.8 Å) using a Gatan Orius 1000 CCD Camera. Two-dimensional (2D) class averaging was performed with the software Relion[122] using on average 30–40 micrographs per sample. The 5 best obtained classes were calculated from around 6000 particles each.

Cryo-electron microscopy

Data collection

3.5 μL of sample were applied to 1.2/1.3 C-Flat (Protochips Inc) holey carbon grids and plunged frozen in liquid ethane with a Vitrobot Mark IV (Thermo Fisher Scientific) (6 s blot time, blot force 0). The sample was observed with a Glacios electron microscope (Thermo Fischer Scientific) at 200 kV. Images were recorded automatically on a K2 summit direct electron detector (Gatan Inc., USA) in counting mode with SerialEM.[123] Movies were recorded for a total exposure of 4.5 s with 40 frames per movie and a total dose of 40 $e^{-}/Å^2$. The magnification was 36,000x (1.15 Å/pixel at the camera level). The defocus of the images was changed between −1.0 and −2.5 μm. Two different datasets have been acquired on the same grid. First, 1040 movies were recorded with stage movement between each hole and then 7518 more movies were recorded with image shifts on a 3x3 hole pattern.

3D reconstruction

The movies were first drift-corrected with motioncor2.[124] The remaining image processing was performed with RELION 3.1.2 [125] and CTF estimation with GCTF.[126] An initial set of particles (box size of 200 pixels, sampling of 2.3 Å/pixel) was obtained by auto-picking with a Gaussian blob. After 2D classification, the best looking 2D class averages were used for a second round of auto picking. Following another 2D classification step, the particles belonging to the best looking 2D class averages were used to create an *ab-initio* starting 3D model which was then used to calculate a first 3D reconstruction with C3 symmetry. The 2D projections from that 3D model were then used for one last auto picking which resulted in a total of 2,582,857 particles. Following another 2D classification and a 3D classification (C1 symmetry, 5 classes) steps, a 3D map at 4.6 Å resolution was obtained from 240,777 particles. The particles were re-extracted (box size of 400 pixels, sampling of 1.15 Å/pixel). After further 3D refinement (C3 symmetry) and 3D classification (C1 symmetry, no alignment, 3 classes) steps, a final set of 126,719 particles was identified which resulted in a 3D reconstruction at 3.6 Å resolution. Refinement of CTF parameters, particle polishing and a second round of CTF parameter's refinement further improved the resolution to 3.4 Å. The resolution was determined by Fourier Shell Correlation (FSC) at 0.143 between two independent 3D maps. The local resolution was calculated with blocres[127] and found to be between 3 and 5 Å. The final 3D map was sharpened with DeepEMhancer.[128]

Model refinement

The atomic model of the S protein in the closed conformation (PDB 6VXX)[11] was rigid-body fitted inside the cryo-EM density map in CHIMERA.[129] The atomic coordinates were then refined with PHENIX.[130] The refined atomic models were visually checked and adjusted (if necessary) in COOT.[131] The final model was validated with MOLPROBITY.[132]

The figures were prepared with CHIMERA and CHIMERAX.[129,133] The data collection and atomic model statistics are summarized in Table S1. The atomic coordinates and the cryo-EM map have been deposited in the Protein Data Bank and in the Electron Microscopy Data Bank under the accession codes 7QIZ and EMD-13776, respectively.

Virus quantification in NHP samples

Upper respiratory (nasopharyngeal and tracheal) and rectal specimens were collected with swabs (Viral Transport Medium, CDC, DSR-052-01). Tracheal swabs were performed by insertion of the swab above the tip of the epiglottis into the upper trachea at approximately 1.5 cm of the epiglottis. All specimens were stored between 2°C and 8°C until analysis by RT-qPCR with a plasmid standard concentration range containing an RdRp gene fragment including the RdRp-IP4 RT-PCR target sequence. SARS-CoV-2 E gene subgenomic mRNA (sgRNA) levels were assessed by RT-qPCR using primers and probes previously described[134,135]: leader-specific primer sgLeadSARSCoV2-F CGATCTCTTGTAGATCTGTTCTC, E-Sarbeco-R primer ATATTGCA GCAGTACGCACACA and E-Sarbeco probe HEX-ACACTAGCCATCCTTACTGCGCTTCG-BHQ1. The protocol describing this procedure for the detection of SARS-CoV-2 is available on the WHO website (https://www.who.int/docs/default-source/coronaviruse/whoinhouseassays.pdf)

Chest CT and image analysis

Lung images were acquired using a computed tomography (CT) system (Vereos-Ingenuity, Philips) as previously described,[50,70] and analyzed using INTELLISPACE PORTAL 8 software (Philips Healthcare). All images had the same window level of −300 and window width of 1,600. Lesions were defined as ground glass opacity, crazy-paving pattern, consolidation or pleural thickening as previously described.[136,137] Lesions and scoring were assessed in each lung lobe blindly and independently by two persons and the final results were established by consensus. Overall CT scores include the lesion type (scored from 0 to 3) and lesion volume (scored from 0 to 4) summed for each lobe as previously described.[50,70]

ELISA

Serum antibody titers specific for soluble native S glycoprotein, FA-cross-linked S (FA-S) and for RBD were determined using an enzyme-linked immunosorbent assay (ELISA). Briefly, 96-well micro titer plates were coated with 1 μg of S, FA-S or RBD proteins at 4°C overnight in PBS and blocked with 3% BSA for 1 h at room temperature after 3 washes with 150 μL PBS Tween-20 0.05%. Serum dilutions were added to each well for 2h at 37°C and plates were washed 5 times with PBS Tween. A horseradish peroxidase (HRP) conjugated goat anti-monkey H+L antibody (Invitrogen) was then added and incubated for 1h before excess Ab was washed out and HRP substrate added. Absorbance was determined at 450 nm. Antibody titers were expressed as ED50 (effective Dilution 50-values) and were determined as the serum dilution at which IgG binding was reduced by 50%. ED50 were calculated from crude data (O.D) after normalization using GraphPad Prism (version 6) "log(inhibitor) vs normalized response" function. ELISA were performed in duplicates.

Protein coupling to luminex beads

Proteins were covalently coupled to Magplex beads (Luminex Corporation) via a two-step carbodiimide reaction using a ratio of 75 μg SARS-CoV-2 S to 12,5 million beads. Magplex beads (Luminex Corporation) were washed with 100 mM mono-basic sodium phosphate pH 6.2 and activated for 30 min on a rotor at RT by addition of Sulfo-N-Hydroxysulfosuccinimide (Thermo Fisher Scientific) and 1-Ethyl-3-(3-dimethylaminopropyl) carbodiimide (Thermo Fisher Scientific). The activated beads were washed three times with 50 mM MES pH 5.0 and added to SARS-CoV-2 S protein, which was diluted in 50 mM MES pH 5.0. The coupling reaction was incubated for 3 h on a rotator at RT. The beads were subsequently washed with PBS and blocked with PBS containing 2% BSA, 3% FCS and 0.02% Tween-20 for 30 min on a rotator at RT. Finally, the beads were washed and stored in PBS containing 0.05% Sodium Azide at 4°C and used within 3 months.

Luminex assay

50 μL of a working bead mixture containing 20 beads per μL was incubated overnight at 4°C with 50 μL of diluted nasopharyngeal fluid. Nasopharyngeal fluids were diluted 1:20 for detection of S-specific IgG and IgA.[70] Plates were sealed and incubated on a plate shaker overnight at 4°C. Plates were washed with TBS containing 0.05% Tween-20 (TBST) using a hand-held magnetic separator. Beads were resuspended in 50 μL of Goat-anti-monkey IgG-Biotin or Goat-anti monkey IgA-Biotin (Sigma Aldrich) and incubated on a plate shaker at RT for 2 h. Afterwards, the beads were washed with TBST, resuspended in 50 μL of Streptavidin-PE (ThermoFisher Scientific) and incubated on a plate shaker at RT for 1 h. Finally, the beads were washed with TBST and resuspended in 70 μL Magpix drive fluid (Luminex Corporation). The beads were agitated for a few minutes on a plate shaker at RT and then readout was performed on the MAGPIX (Luminex Corporation). Reproducibility of the results was confirmed by performing replicate runs.

Pseudovirus neutralization assay

Pseudovirus was produced by co-transfecting the pCR3 SARS-CoV-2-SΔ19 expression plasmid (Wuhan Hu-1; GenBank: MN908947.3) with the pHIV-1NL43 ΔEnv-NanoLuc reporter virus plasmid in HEK293T cells (ATCC, CRL-11268).[115] The pCR3 SARS-CoV-2-SΔ19 expression plasmid contained the following mutations compared to the WT for the variants of concern: deletion (Δ) of H69, V70 and Y144, N501Y, A570D, D614G, P681H, T716I, S982A and D1118H in B.1.1.7 (Alpha, UK); L18F, D80A, D215G, L242H, R246I, K417N, E484K, N501Y, D614G and A701V in B.1.351 (Beta, SA); L18F, T20N, P26S, D138Y, R190S, K417T, E484K, N501Y, D614G, H655Y and T1027I in P.1 (Gamma, BR).[115]

HEK293T/ACE2 cells kindly provided by Dr. Paul Bieniasz[119] were seeded at a density of 20,000 cells/well in a 96-well plate coated with 50 μg/mL poly-L-lysine 1 day prior to the start of the neutralization assay. Heat-inactivated sera (1:100 dilution) were serial

diluted in 3-fold steps in cell culture medium (DMEM (Gibco), supplemented with 10% FBS, penicillin (100 U/mL), streptomycin (100 μg/mL) and GlutaMax (Gibco)), mixed in a 1:1 ratio with pseudovirus and incubated for 1 h at 37°C. These mixtures were then added to the cells in a 1:1 ratio and incubated for 48 h at 37°C, followed by a PBS wash and lysis buffer added. The luciferase activity in cell lysates was measured using the Nano-Glo Luciferase Assay System (Promega) and GloMax system (Turner BioSystems). Relative luminescence units (RLU) were normalized to the positive control wells where cells were infected with pseudovirus in the absence of sera. The neutralization titers (ID_{50}) were determined as the serum dilution at which infectivity was inhibited by 50%, respectively using a non-linear regression curve fit (GraphPad Prism software version 8.3). Notably, this pseudovirus neutralization assay revealed an excellent correlation with authentic virus neutralization on a panel of human convalescent sera.[115]

Antigen specific T cell assays using non-human primate cells

To analyze the SARS-CoV-2 protein-specific T cell, 15-mer peptides (n = 157 and n = 158) overlapping by 11 amino acids (aa) and covering the SARS-CoV-2 Spike sequence (aa 1 to 1273) were synthesized by JPT Peptide Technologies (Berlin, Germany) and used at a final concentration of 2 μg/mL.

T-cell responses were characterized by measurement of the frequency of PBMC expressing IL-2 (PerCP5.5, MQ1-17H12, BD), IL-17a (Alexa700, N49-653, BD), IFN-γ (V450, B27, BD), TNF-α (BV605, Mab11, BioLegend), IL-13 (BV711, JES10-5A2, BD), CD137 (APC, 4B4, BD) and CD154 (FITC, TRAP1, BD) upon stimulation with the two peptide pools. CD3 (APC-Cy7, SP34-2, BD), CD4 (BV510, L200, BD) and CD8 (PE-Vio770, BW135/80, Miltenyi Biotec) antibodies was used as lineage markers. One million of PBMC were cultured in complete medium (RPMI1640 Glutamax+, Gibco; supplemented with 10% FBS), supplemented with co-stimulatory antibodies (FastImmune CD28/CD49d, Becton Dickinson). The cells were stimulated with S sequence overlapping peptide pools at a final concentration of 2 μg/mL. Brefeldin A was added to each well at a final concentration of 10 μg/mL and the plate was incubated at 37°C, 5% CO2 during 18 h. Next, cells were washed, stained with a viability dye (LIVE/DEAD fixable Blue dead cell stain kit, ThermoFisher), and then fixed and permeabilized with the BD Cytofix/Cytoperm reagent. Permeabilized cell samples were stored at -80 °C before the staining procedure. Antibody staining was performed in a single step following permeabilization. After 30 min of incubation at 4°C, in the dark, cells were washed in BD Perm/Wash buffer then acquired on the LSRII cytometer (Beckton Dickinson). Analyses were performed with the FlowJo v.10 software. Data are presented as the sum of each peptide pool and the non-stimulated (NS) condition was multiplied by two.

Statistical analysis

Statistical significance between groups was performed using Graphpad Prism (v9.2.0). Differences between unmatched groups were compared using an unpaired Mann–Whitney U test (significance $p<0.05$), and differences between matched groups were compared using Wilcoxon signed-rank test ($p<0.1$). Statistical analysis of NHP gRNA and sgRNA were carried out using Mann-Whitney unpaired t-test in GraphPad Prism software (v8.3.0).